Supernova cosmology: legacy and future

ARIEL GOOBAR

The Oskar Klein Center, Physics Department, Stockholm University, AlbaNova University Center, SE 106 192 Stockholm, Sweden, ariel@fysik.su.se

BRUNO LEIBUNDGUT

European Southern Observatory, Karl-Schwarzschild-Strasse 2, 85748 Garching, Germany

and

Excellence Cluster Universe, Technische Universität München,

Boltzmannstrasse 2, 85748 Garching, Germany, bleibund@eso.org

Abstract The discovery of *dark energy* by the first generation of high-redshift supernova surveys has generated enormous interest beyond cosmology and has dramatic implications for fundamental physics. Distance measurements using supernova explosions are the most direct probes of the expansion history of the Universe, making them extremely useful tools to study the cosmic fabric and the properties of gravity at the largest scales. The past decade has seen the confirmation of the original results. Type Ia supernovae are among the leading techniques to obtain high-precision measurements of the dark energy equation of state parameter, and in the near future, its time dependence. The success of these efforts depends on our ability to

understand a large number of effects, mostly of astrophysical nature, influencing the observed flux at Earth. The frontier now lies in understanding if the observed phenomenon is due to vacuum energy, albeit its unnatural density, or some exotic new physics. Future surveys will address the systematic effects with improved calibration procedures and provide thousands of supernovae for detailed studies.

CONTENTS

1 Introduction

Particle physics and cosmology are tightly linked and ideally complement each other. The physics of the early universe is beyond the reach of even the most powerful accelerators and needs to be deduced from the embers left by the Big Bang. The richness of the cosmic microwave background radiation as a source of information of the early universe has been described many times and has to be counted amongst the most successful scientific endeavors of the past two decades [1–3]. Observational cosmology can now address particle physics questions, e.g. the number of neutrino species and the sum of their masses, beyond the Standard Model particles as dark matter candidates, and even braneworld scenarios invoking extra spatial dimensions. Theoretical high-energy physics has started to address questions concerning the uniqueness of the observable universe and String Theory inspired models to explain the current state of the cosmos [4,5]. Supernovae, the violent destruction of an entire star, offer means to obtain accurate information about the expanding universe, and are therefore a precious instrument in the cosmology tool box. These luminous explosive events are important for modern cosmology since they can be detected even in very remote galaxies.

Furthermore, some subtypes, Type Ia supernovae (SNe Ia) in particular, can be calibrated fairly reliably to provide accurate distances that can be used to map the expansion history of the universe.

The current expansion rate, the Hubble constant H_0, was determined with supernova distances for several decades [6–8]. Two different methods have been employed using supernovae. Assuming a unique luminosity for SNe Ia, often referred to as the "standard candle" method, one can directly use the observed brightness to infer the distance, an appealing technique due to its simplicity. Various (astrophysical) effects influence the distance measurement, but through suitable calibration and corrections this remains very successful. The other method is to measure the physical expansion of a Type II supernova through the radial velocity and its brightness increase reflecting the growth in surface area. This method has been applied to supernovae stemming from massive stars and with extended envelopes. In the local universe, this measurement is still possible, but due to the limited luminosity of the Type II supernovae becomes very difficult with current observing facilities at larger distances [9].

Dark Energy, detected using SNe Ia through the accelerated expansion of the universe, is amongst the most notorious recent additions to our understanding of the cosmic composition (e.g. [10–14]). After the first indications based on only small samples of supernovae [15, 16] the past decade has seen a significant amount of telescope time invested in further refining our understanding of SNe Ia and their ability as distance indicators. The cosmological results have been confirmed and the uncertainties have decreased dramatically due to better controlled observational techniques, improved calibrations, larger samples and an extended redshift range. The current studies are limited by the systematic uncertainties re-

lated to the supernova explosions and the light propagation through the universe rather than the size of the statistical sample. Overall, there are now several hundred Type Ia supernovae available for cosmic distance measurements and there are prospects to increase these numbers at least ten fold within the next decade. The field has moved from the discovery of dark energy to its first characterization through the measurement of the equation of state parameter, $w = p/\rho c^2$, i.e., the ratio between pressure and energy density when treated as a fluid. Future projects will address potential time-dependence of this parameter, $w(t)$. Note that from now on, we will use natural units, i.e., $c = 1$, unless stated otherwise.

Although there is no observation today that is incompatible with Einstein's cosmological constant, Λ, being responsible for the accelerated expansion of the universe, only few high-energy physics theorists are ready to quit searching for alternative models.

A cosmological constant ($w = -1$) can be naturally associated with the vacuum zero-point energy predicted by quantum field theory. However, the corresponding density, $\rho_{vac} \sim (10^{-3}\text{eV})^4$, does not match any particle physics scale, and is more than 120 order of magnitudes lower than the "natural" scale set by the Planck mass, $M_P^4 \sim (10^{28}\text{eV})^4$ or about 60 orders of magnitude below the supersymmetry breaking scale, $M_{SUSY}^4 \sim (10^{12}\text{eV})^4$. Furthermore, it may be regarded as a great coincidence that ρ_{vac} and ρ_M, are so close in spite of $\rho_M \propto a^{-3}$, i.e., the density of non-relativistic matter gets diluted proportionally to the growing volume of the expanding universe, while the vacuum energy density remains constant.

Some highly regarded physicists have invoked the Anthropic principle to elude these difficulties arguing that we are witnessing the result of a selection process: galaxies, stars, planets and intelligent beings would only have a chance to come

to being in "un-natural" universes like ours [17, 18]. Another common view on this problem is that a yet unknown mechanism sets the vacuum energy to zero and the present day acceleration is instead caused by new physics, e.g., a light scalar field or an effective change of gravity at the largest scales in a higher dimension universe. While the Anthropic hypothesis cannot be further tested experimentally (with a possible exception described in [19]), we will not address it further here. Alternatives to Λ, however, would imply that the dark energy density would change in time (and space), something that can be tested with SNIa, especially when combined with other probes. In particular, measurements of the expansion history and growth of structure in a universe with dynamically evolving dark energy would lead to $w(t) \neq -1$, i.e., distinguishable from Λ.

A new generation of multi-probe projects are being planned, and their relative merits have been assessed by the ESA–ESO Working Group on *Fundamental Cosmology* [20] and the *Dark Energy Task Force* report [21]. These forthcoming measurements are expected to provide the first accurate measurements of the time dependence of w.

The use of supernovae for cosmology has been reviewed many times. The original cosmological application of supernovae was for the Hubble constant [7, 8, 22]. The connection of supernovae with Dark Energy has been described in many reviews as well [10, 12, 23–25]. Using supernovae to map the cosmic distance scale requires a sufficient understanding of the explosions and the astrophysical effects, which affect light propagation. These are very important considerations for the derivation of accurate distances.

1.1   Supernova classification

Supernovae have been recognised as an own class of astrophysical objects by Baade and Zwicky [26] following earlier work by Lundmark [27], who noted that there is a class of eruptive variable objects, which are about 10 magnitudes (i.e. 10000 times) more luminous than regular (and more frequent) novae. An early classfication scheme for supernovae was introduced by Minkowski [28, 29].

Supernova classification is based on their spectral appearance near maximum light [30]. The Type II supernovae show hydrogen in their maximum-light spectrum, while Type I supernovae lack hydrogen. Type Ib SNe display prominent helium lines, while the Type Ic display neither hydrogen nor helium. Type Ia supernovae spectra are dominated by lines from higher-mass elements, like calcium, sulphur, silicon and iron, but lack hydrogen and helium - the most abundant elements in the universe.

The past years have seen some interesting modifications to the classification after several decades of relative few new additions [29, 31]. Several examples of objects, which do not fit any of the established classes have been added. The Type Ia class is overall very uniform in its appearance, but shows some spread in its luminosity and spectral evolution. Both overluminous and underluminous SNe Ia have been identified (e.g. [14]). In particular, a range of expansion velocities – as derived from the absorption trough of several lines (e.g. [32–35]) has been established. These peculiar objects typically show interesting, and sometimes subtle, deviations in their spectral appearance, which may allow to refine their use as distance indicators (see Sec. 5). Thanks to the large number of SN surveys conducted over the past decade, a small number of truly different objects has been discovered. Among them are objects, which appear very close to SNe Ia,

but displayed a strong hydrogen emission (SN 2002ic; [36]), extremely luminous objects with rather slow expansion velocities (SN 2003fg; [37], SN 2006gz; [38], SN 2009dc; [39]), and extremely faint objects (SN 2000cx; [40], SN 2002cx; [41], 2005hk; [42], 2008ha; [43], but see [44] for a differing view on the classification of this object). In many cases, the peculiar nature of these objects only became clear through a detailed analysis of the pre-maximum color and spectral evolution or the late phase evolution. It should be noted that the majority (70% in a volume-limited sample and 77% in a magnitude-limited sample) of SNe Ia are quite homogeneous and only a few objects are true outliers [45].

The simple classification scheme of maximum light spectra has to be expanded to include various additional parameters (color, light curve shapes, etc.) for a complete description of the supernovae. The coming years, with many large supernova surveys planned (Sec. 5), will provide the detailed data to define additional classification criteria.

Several major samples of supernovae have been assembled in the past two decades. Leibundgut [46] provided an overview of the situation a decade ago. In the meantime, the Center for Astrophysics supernova program has produced an impressive sample of around 160 nearby SNe Ia [47], the Lick Observatory Supernova Search has assembled several hundred SNe Ia and has published a first set recently [48], the Carnegie Supernova Project has also collected a fairly large number of nearby SNe Ia with both optical and near-infrared data [49]. The SNfactory has implemented a bold new technique for the study of super-novae: rather than carrying out a series of photometry measurements in individual broadband filters, SNfactory uses an integral field spectrograph to create synthesized photometry corresponding to any possible optical filter set. The

Palomar Transient Factory [50] and the PanSTARRS supernova searches have started and have already produced a number of interesting objects. The distant searches will be described in Sec. 7. The nearby supernovae are critical for the cosmology as they provide the comparison sample and also the anchoring point of the distance scale.

1.2   Supernova physics

The display of a supernova is the result of the explosion mechanism and the structure of the exploding star. Collapsing about one solar mass from the radius of the Sun to a neutron star or a black hole releases about 10^{46} J, mostly in neutrinos. About 10^{-2} of this energy goes into the acceleration of the stellar material and 10^{-4} into radiation (10^{42} J). The energy gain of burning about one solar mass to iron-group elements due to the higher nuclear binding energy also is around 10^{42} J. Hence the two mechanisms produce very similar luminosities.

Type II and Type Ib/c SNe are associated with core-collapse supernovae of massive stars [51], while the Type Ia supernovae most likely are due to the thermonuclear explosion of a compact white dwarf star [52].

1.2.1   THERMONUCLEAR EXPLOSIONS   The similarity between SNIa has been linked to a threshold phenomenon involving at least one white dwarf accreting mass from the surrounding environment. These compact remnants of low mass stars emit only thermal radiation from their slow gravitational contraction.

Thermonuclear explosions are due to the explosive burning of carbon and oxygen. The energy released from the synthesis of iron-group elements is mostly used to overcome the binding energy to disintegrate the star. The fairly quick brightness evolution (light curve) of Type Ia supernovae (see Fig. 1), a rise time

to maximum light of about 17 to 20 days and a rapid decline after peak indicates a small progenitor star.

The temperatures and densities for carbon burning are reached shortly before the Chandrasekhar-mass, the highest mass a non-rotating white dwarf can obtain before gravity overcomes the electron degeneracy and collapses the white dwarf. Due to the electron degeneracy the mass-radius relation is inverted and the more massive white dwarfs actually have smaller radii. Once the carbon burning is triggered, it starts a simmering phase within the star, which can last several hundred years. During this phase the burning creates a large instability, which at some point turns into a runaway (e.g. [52]). At this point the burning proceeds through the star very rapidly and disrupts it completely within seconds (e.g. [53]). There are two ways the burning front can move through the star: at subsonic speeds, called a deflagration, or at supersonic velocity, designated detonation. Pure deflagrations typically have the problem that they do not achieve enough energy for the bright display of Type Ia SNe, but they have been suggested for several of the less luminous SNe Ia. Detonations have been disfavored for many years as they burn most of the star to iron-group elements and do not leave a significant amount of intermediate-mass elements, like silicon, calcium and sulphur observed in the spectra. Models with a transition from deflagration to detonation have been favored. In this case, the subsonic burning front accelerates to reach supersonic speed in the outer layers and hence provides a mix of iron-group and intermediate-mass elements. The exact reason for the transition, however, has not been completely identified.

Mass accretion is critical in this scenario. The white dwarf can only grow in mass, if it receives matter from a companion star. This immediately requires

a close binary stellar system. Also, the white dwarf needs to grow to close to the Chandrasekhar mass ($\sim 1.4 M_\odot$), which is not easy given that typical white dwarfs are normally below a solar mass. Possible accretion scenarios, both with significant problems at the moment, are either the merging of two white dwarfs (e.g. [54] for at least sub-luminous SNe Ia) or mass loss from the nearby companion star. There are observational arguments for both these channels. A further option is to trigger the explosion well below the Chandrasekhar mass by explosive burning of surface material. In such a case, helium detonates near the surface, possibly where the accretion reaches the white dwarf, and then triggers the central carbon explosion by pressure waves focussing near the center. While this possibility has for a long time been regarded as producing the wrong nucleosynthesis, it has recently been revived in full 3-dimensional simulations [55, 56].

The optical display of a Type Ia supernova comes from the radioactive decay of newly synthesized material. Adiabatic cooling of the ejecta means that there is no remnant energy for optical emission. Instead the decay chain from ^{56}Ni$\rightarrow^{56}$Co$\rightarrow^{56}$Fe (e.g. [57]) is responsible for powering the light curve. The radiation transport in Type Ia supernovae is very complicated as the original $\gamma-$rays from the radioactive decay are down-scattered to lower energies. This happens mostly through Compton scattering and then absorption and line emission in local atoms (e.g. [58]). This non-thermal process is extremely difficult to model and depends on complete atomic data for many ionized atoms. The emission at different wavelengths is modulated by these radiation transport effects. A striking example is the secondary peak, which is observed in the light curves of red and infrared filters (at $\lambda \geq 700$nm, see Fig. 1). This has been tentatively explained as due to the ionisation state of iron [59], where the opacities change

dramatically for doubly- to singly-ionised iron.

The original hopes of a single explosion mechanism for all SNe Ia is probably no longer tenable. The observed diversity indicates that several of the evolutionary scenarii and also explosion mechanisms are at work. It has also emerged that the explosions are unlikely to be spherical and hence viewing angle effects need to be taken into account as well [60]. In particular, they can introduce a natural scatter into the observables.

Critical observational input to the models would be the total mass of the explosion, the newly synthesized ^{56}Ni mass and the explosion energy (e.g. [61]). This information is difficult to come by and is being assembled only slowly.

1.3   Supernova rates

Supernovae are rare objects. The last millennium has only six confirmed supernovae in our own Milky Way and SN 1987A in the Large Magellanic Cloud. The local rate of Type Ia supernovae is about $3 \cdot 10^{-5}$ SNe Ia Mpc^{-3}yr^{-1} [62, 63]. The past decade has seen the industrialization of sky monitoring and supernovae are now found regularly. The challenge is different for nearby and distant supernovae. Due to the limited volume it is rather difficult for find nearby supernovae as large sky areas need to be monitored. Nevertheless, the rate of supernova discoveries in the local volume (out to about 100 Mpc) has doubled in the past decade. For higher redshifts, the increase has been much larger due to the larger mirror/longer exposures and wide-area capabilities, since distant supernovae are found by deep pencil-beam searches. Due to the great depth, a large volume is searched and many supernovae are found.

The SN Ia rate is connected to the star formation of the local galaxy and

can also provide information on the gestation time before a supernova explosion occurs. The progenitor systems of SNe Ia have not been uniquely identified and hence the rate as a function of redshift (or look-back time) provides important clues. For systems, which take a long time to grow the white dwarf towards the Chandrasekhar mass (several 10^9 years) there has to be a cutoff when the universe is not old enough to produce a Type Ia supernova. Figure 2 displays the current state of affairs. There is clearly an increase by a factor of 3 in the SN Ia rate back to a redshift of 1. If the drop for z>1 is real then we may see the onset of the first supernovae at that time.

Searches at very high redshifts are currently under way (as part of the CLASH and CANDELS HST multi-cycle projects). They will show whether indeed there are no Type Ia supernovae at $z = 2$ (about 3 billion years after the Big Bang for the canonical cosmological parameters.

2 Standard cosmology

Modern cosmology is based on Einstein's field equations of General Relativity (GR):

$$R_{\mu\nu} - \frac{1}{2}g_{\mu\nu}R = 8\pi G T_{\mu\nu} + \Lambda g_{\mu\nu}, \tag{1}$$

which connects spatial curvature (left hand side) and energy content (right hand side). Equation 1 includes the extra term Λ, also called the *cosmological constant*, that Einstein introduced in 1917 to account for the possibility that, on the largest scales of the universe, the attractive nature of gravity could be neutralized, thus potentially allowing for a static solution. In the context of quantum field theory, a Λ term arises naturally as a vacuum energy density, $\rho_{vac} = \frac{\Lambda}{8\pi G}$, i.e. the zero-point energy associated with the production and annihilation of all virtual

particles.

2.1   Friedmann-Lemaître models

To compute cosmological observables from GR, Eq. (1) is solved using two simpli-

fying assumptions about the universe: *homogeneity* and *isotropy* over very large

scales. Expressed in the Robertson-Walker line element, distances in space-time

become $(c = 1)$:

$$ds^2 = dt^2 - a(t)^2 \left(\frac{dr^2}{1 - kr^2} + r^2 d\theta^2 + r^2 \sin^2 \theta d\phi^2 \right), \tag{2}$$

where $a(t)$ is scale factor of the expanding universe and k indicates the curvature:

$(0, 1, -1)$ for a flat, closed or open universe.

The solutions to the temporal and spatial components of the Einstein's field

equations in the Robertson-Walker metric lead to two fundamental equations for

the dynamics of the universe first found by Friedmann and Lemaître for the first

and second derivative of the scale factor, a:

$$\left(\frac{\dot{a}}{a} \right)^2 = \frac{8\pi G}{3} \rho - \frac{k}{a^2} \tag{3}$$

and

$$\frac{\ddot{a}}{a} = -\frac{4\pi G}{3} (\rho + 3p), \tag{4}$$

where ρ and p are the energy density and pressure of the cosmic fluids, and are

typically related through the equation of state parameter as:

$$p = w \cdot \rho \tag{5}$$

Since the discovery of the expansion of the universe in the late 1920's, the

current expansion rate is called the Hubble constant, $\frac{\dot{a}}{a} = H_0$. The goal of

observational cosmology since then, is to measure the time dependence of the expansion rate, $H(t)$, thus indirectly probing the contents of the universe.

2.2 Components in the Friedmann-Lemaître cosmological models

In the Standard Model of cosmology, the universe has been expanding and cooling since almost 14 billion years ($\sim H_0^{-1}$). Thus, after the initial "Big Bang", the energy content of the universe was dominated by relativistic particles ($w = 1/3$), eventually surpassed by non-relativistic matter ($w = 0$) as the temperature fell well below the mass of standard model particles.[1]

A continuity equation can be derived from Eqs. (3-5):

$$\dot{\rho} + 3H\rho(1 + w) = 0 \tag{6}$$

The density of cosmic fluids in the expanding universe evolves according to Eq. (6) as:

$$\rho = \rho_0 e^{3 \int_{a_0}^{a} \frac{1+w}{a'} da'}, \tag{7}$$

where a_0 is the scale factor today.

A simple relation is thus found for fluids with *constant w*:

$$\rho = \rho_0 \left(\frac{a_0}{a}\right)^{3(1+w)}. \tag{8}$$

We thus find the familiar dilution for non-relativistic matter as the universe expands, $\rho_M = \rho_M^0 \left(\frac{a_0}{a}\right)^3$, and because of redshift, by another power of a for

---

[1] A convenient relation between age of the universe and the plasma temperature in the early universe is $T(\text{MeV}) = t^{-\frac{1}{2}}(\text{s})$.

relativistic matter $\rho_R = \rho_R^0 \left(\frac{a_0}{a}\right)^4$. Since Λ is constant, is is directly seen from Eq. (8) that its equation of state is $w_\Lambda = -1$. More generically, any dominant fluid with $w < -1/3$ will cause the universe to accelerate, as seen from Eq. (4). Such fluids are called *dark energy*, the "simplest" one being the vacuum energy density associated with the cosmological constant, Λ. Other dark energy candidates are discussed in e.g. [5, 13].

It is customary to re-write the Friedmann equation (3) in terms of the cosmological redshift, $1 + z = \frac{a_0}{a}$, and the density terms normalized by the critical density corresponding to a flat universe, $\Omega_{DE} = \frac{\rho_{DE}}{\rho_c} = \rho_{DE} \cdot \frac{8\pi G}{3H_0}$, and the curvature term is defined as $\Omega_K = -k(a_0 H_0)^{-2}$.

Since we lack the knowledge of the nature and properties of the equation of state of dark energy, phenomenological parameterizations of $w(z)$ are used for comparisons with data, e.g.

$$w(z) = w_0 + w_a \left(1 - \frac{a}{a_0}\right) = w_0 + w_a \frac{z}{1 + z}, \tag{9}$$

where the free parameters w_0 and w_a are fitted with observational data.

2.3 The luminosity distance and the Hubble diagram

There are several cosmological distances measures. Here we concentrate on the *Luminosity Distance*, d_L, which is defined from the expected flux, $\mathcal{F}$, from an object with luminosity L (in units of energy per unity time and unit area), $\mathcal{F} = \frac{L}{4\pi d_L^2}$. Since the universe expands, any cosmological distance estimate will depend on the growth of the scale factor and thus on the Hubble parameter. For a full derivation, the reader should consult a cosmology text book, e.g. [68]. Here we concentrate on the final expression (neglecting the radiation density term $\Omega_R \sim 10^{-5}$):

$$d_L = \begin{cases} (1+z)\frac{1}{\sqrt{-\Omega_K}}\sin(\sqrt{-\Omega_K}\,I), & \Omega_K < 0 \\[2mm] (1+z)\,I, & \Omega_K = 0 \\[2mm] (1+z)\frac{1}{\sqrt{\Omega_K}}\sinh(\sqrt{\Omega_K}\,I), & \Omega_K > 0 \end{cases} \tag{10}$$

$$\Omega_K = 1 - \Omega_M - \Omega_{DE}, \tag{11}$$

$$I = \int_0^z \frac{dz'}{H(z')}, \tag{12}$$

$$H(z) = H_0\sqrt{(1+z)^3\,\Omega_M + f(z)\,\Omega_{DE} + (1+z)^2\,\Omega_K}, \tag{13}$$

$$f(z) = \exp\left[3\int_0^z dz'\,\frac{1+w(z')}{1+z'}\right]. \tag{14}$$

It is customary to use logarithmic distances in astronomy, the *distance modulus*, $\mu = 5\log_{10} d_L(\mathrm{Mpc}) + 25 = m_f - M_f$, where the last term corresponds to the difference between the measured magnitude of the object, m_f and its absolute magnitude through the same filter f, M_f, i.e. corresponding to the flux of the object if placed 10 pc away from the observer. Cosmological model testing is done by comparing measured distance moduli *vs.* redshift against model predictions. This is usually called the Hubble diagram. The supernova Hubble diagram, which will be discussed in more detail in the following is displayed in Fig. 3.

3 Cosmology with Type Ia supernovae

Since SNe Ia display rather uniform light curves, they can be used as local clocks. This test for cosmological time dilation had been proposed soon after supernovae were recognized and was implemented with the first distant supernovae [70, 71]. The spectral evolution also tests for this stretching of time in the observer frame [72]. All tests so far have confirmed the prediction of general relativity. The corrections for time dilation are now routinely applied to the supernova data.

Most supernova searches operate by repeated imaging of patches of the sky

with many thousand galaxies. Supernovae are found through pixel-by-pixel sub-
tractions of CCD images obtained at different epochs, as shown in Figure 4.

Once a supernova is detected, a few steps are necessary before the brightness
can be used for distances estimates. First and foremost, the object is spectro-
scopically classified, as described in Sec. 1.1. The spectrum also provides the vital
redshift for the object. In many cases light from the host galaxy can be analyzed
to find a redshift, but for "hostless" supernovae (where the surface brightness of
the host galaxy falls below the detection limit) the redshift can also be determined
from the supernova spectrum itself. Figure 5 shows the identification spectra of
two Type Ia supernovae, SN2003du in the nearby universe, and SN2000fr at
$z = 0.543$, i.e., more than 8 Gyrs apart. The striking spectral similarity is the
key of the "standard candle" technique. Since distances are established based
on the peak flux, light curves are built through several filters, ideally including
observations well before and after maximum, as shown in Fig. 1. Besides time
dilation making the light curve width increasingly broader with redshift, SNIa
optical light curves exhibit a range in widths. The correlation between light curve
and supernova luminosity has been established over several years. More luminous
supernovae display typically a slightly slower evolution.

Intervening dust can scatter and absorb supernova light and hence produce a
dimming, which needs to be corrected for the distance measurement. Additional
effects may also influence the observed colors of SNIa, as discussed in Section 5.
Several light curve "fitters" have been proposed to extract the key parameters
from the data: the day of maximum and the corresponding peak flux, the light
curve shape, and the reddening (color excess). The latter is often computed as the
relative magnitude attenuation between the restframe B-band and the V-band.

The empirical *color-brightness* and *lighcturve shape-brightness* relations used to "standardize" SNe Ia are shown in Fig. 6.

Since the measurements are done with fixed filter pass-bands, irrespectively of the supernova redshift, the measured fluxes correspond to different parts of the restframe spectrum. The distance estimates rely on flux ratios of the same restframe filters and hence, a K-correction is needed to transfer the observed flux into the restframe for comparison with local objects. Due to the significant spectral evolution, high S/N spectroscopic observations would be needed for every flux point, a daunting task! However, given the uniformity of SNe Ia, spectral *templates* are used to compute K-corrections. These templates are made of well sampled, low noise, measurements of SNe Ia, mostly at low redshift. Any potential reddening is determined by comparison of the multi-band data with synthetic colors calculated from spectral templates after applying an extinction law, e.g., the one found for stars in the Milky Way [76]. The photometric measurements from different telescopes also need to be corrected for differences in the wavelength response of the telescope reflectivity and instrument sensitivity. Modern analysis methods try to correct for these systematic effects in the light curve fitting.

To summarize, observed SN peak magnitudes at redshift z through a filter Y are compared with model predictions taking into account the observed color and light curve shape (c, s). The effect of cosmological redshift on the spectrum, from the restframe wavelength X to the observations in Y are handled through the cross-filter K_{XY}-corrections [77]. These would typically also include effects from reddening and light curve shape.

$$m_Y(z, d, c) = M_X(s) + 5 \log_{10} d_L(z) + K_{XY}(z, s, c) + A_Y^{MW}, \qquad (15)$$

where the last term corresponds to dimming by Milky-Way dust. Note that in Eq. (15) it is implicitly assumed that corrections for extinction in the host galaxy are included in K_{XY}.

3.1 The Hubble constant

As discussed in Sec. 2.3, the relation between the distance modulus and cosmological redshift can be used to measure cosmological parameters such as H_0, Ω_M, Ω_{DE} and the dark energy equation of state parameter, w. For $z \ll 1$, we find from Eq. (14):

$$d_L = \frac{cz}{H_0} \left(1 + \frac{1}{2}(1 - q_0)z + \mathcal{O}(z^2) \right), \qquad (16)$$

where we have explicitly reinserted the speed of light c into the expression and introduced the deceleration parameter, q_0, which is related to the cosmological "fluids" as:

$$q_0 = -\left(\frac{\ddot{a}}{a} \right) \frac{1}{H_0^2} \qquad (17)$$

$$= \sum_i \frac{\Omega_i}{2} \left(1 + 3 \frac{p_i}{\rho_i c^2} \right). \qquad (18)$$

The linear part of the Hubble diagram, $d_L(z \ll 1) \approx cz/H_0$, has been used to measure H_0 since several decades using magnitude measurements to SNIa using optical data, e.g., through the B-band filter, m_B:

$$\mu = m_B - M_B = 5 \log cz - 5 \log H_0 + 25 + K_{BB} + A_B^{MW}. \qquad (19)$$

Thus, $\log H_0$ can be read off from the intercept of the $\log cz - 0.2 m_B$ relation (cf. Fig. 3).

While SNe Ia are very useful for measuring relative distances, extracting H_0 requires an absolute calibration of the SNIa brightness. Since theoretical models are not sufficiently accurate, the SNIa absolute magnitude needs to be calibrated observationally [22]. Cepheid stars are used to measure distances to galaxies in the nearby universe. By now, Cepheid distances to 15 SNIa host galaxies within about 20 Mpc have been obtained with the *Hubble Space Telescope* [78]. Riess *et al.* [79] mitigated some of the shortcomings in building up the *distance ladder* to obtain absolute distances to SN Ia hosts. Near-IR observations of Cepheids in six systems with accurate SN Ia data were used to improve the calibration and reducing the uncertainty from extinction by dust. Furthermore, a better anchoring system was found to calibrate the Cepheid distances, the "maser" galaxy NGC 4258, for which an accurate absolute distance can be derived. Riess *et al.* [79] report $H_0 = 74.2 \pm 3.6$ km s^{-1}Mpc^{-1}, where the 4.8 % error includes systematic uncertainties.

3.2 The accelerated expansion

The extension of the SNIa Hubble diagram to higher redshifts, needed to probe the change in the cosmic expansion rate, requires a specific observational strategy: large patches of the sky need to be scanned regularly. This prompted the need for medium size telescopes, $2-4$ meters in diameter, equipped with CCD cameras with large fields of view.

By the mid-nineties, Goobar & Perlmutter [80] showed that constraining the value of the cosmological constant, Λ, was feasible using SNIa data, if the surveys targeted a wide range of redshifts, thereby allowing to break the degeneracy in cosmological parameters.

Figure 7 shows the $\Omega_M - \Omega_\Lambda$ plane, with the two original results of the SCP [16] and HZ SN Team [15], along with the recent Union2 compilation based on 557 SNIa [69]. The data-set includes 192 SNe with $z \leq 0.15$ from [47, 81–84]. The intermediate and high-z includes samples from [15,16,73,85–92], adding up to 106 objects with $0.15 < z \leq 0.55$, 64 with $0.55 < z \leq 0.75$, 41 with $0.75 < z \leq 0.95$ and 28 SNIa with $z > 0.95$. The SN contours are derived from the Hubble diagram data shown in Figure 3.

4   Cross-cutting techniques

The power of the SNIa data for constraining cosmological parameters is vastly enhanced when the likelihood functions are combined with what is found with other probes, most notably the cosmic microwave background (CMB) anisotropies and baryon acoustic oscillations (BAO), as shown in Figure 7 and discussed in [12]. The combination of the different techniques becomes dramatically clear in the determination of w. For this measurement all methods show large degeneracies, but their combination provides a powerful tool to constrain a constant w, as shown in Fig. 8.

Similarly to the use of SNIa as "standard candles" for distance estimates, the CMB and BAO techniques rely on "standard rulers". Matter-radiation oscillations with wavelengths given by the product of the sound speed and the elapsed time since the Big Bang leave a characteristic bump in the power spectrum of the CMB temperature fluctuations originating at $z \sim 1100$ and corresponding to an angular scale of about $1°$ on the sky today. Measurement of this angular scale in WMAP 7-year data [94] leads to the precise constraints cosmological parameters, as shown in Figs. 7 and 8. As the universe expands and photons decouple

from baryons, the matter anisotropies grow into the structures observed today, down to the scale of galaxies and clusters of galaxies. By studying a sample of Luminous Red Galaxies in the SDSS survey, Eisenstein *et al.* [95] could measure the ~ 150 Mpc length of the "ruler" at $z \sim 0.35$ leading to significant parameter constraints, mainly on Ω_M.

Whereas the SNIa Hubble diagram is anchored at $z \approx 0$, the CMB and BAO originate in the early universe. As a result, the "orientation" of the confidence regions differ between the techniques, thus rendering the crossing of the allowed regions particularly useful to derive accurate cosmological parameters.

5   The era of precision cosmology

The pioneering efforts by the SCP (led by Saul Perlmutter) and the High-Z team (led by Brian Schmidt) in the mid and late 90's were followed by new SN programs which developed the field in several directions.

Two major programs were established to collect large samples of high quality data in the $z = [0.3 - 1]$ redshift range: the ESSENCE program at the CTIO 4-m in Chile [96] and SNLS at the 3.6-m CFHT in Hawaii [89]. These programs were backed up with significant spectroscopic identification efforts from $8 - 10$ meter class telescopes: VLT, Keck, Gemini and Magellan. The 3-year SNLS sample recently reported by [97] includes over 250 SN Ia, i.e., about 180 additional supernovae to what is already included in the Union2 sample. SNLS and ESSENCE have additional $\sim$300 SNe Ia unpublished so far.

One of the observational breakthroughs of SNLS was introducing the "rolling search" technique. One-square-degree fields were revisited every 4 to 5 nights in multiple bands, thus new objects were found while light curves were built of

previously discovered supernovae. The excellent time sampling with several filters and with a single telescope and CCD system dramatically improved the quality of the SN light curves.

The redshift "gap" around $z \sim 0.2$ is filled by the SDSS-II supernova survey. The first data [98] includes 103 SNe Ia with redshifts $0.04 < z < 0.42$. Overall, it is expected that the SDSS-II supernova survey has about 400 supernovae for the analysis.

Finally, the Hubble diagram is anchored with supernovae from the Calan-Tololo [81] and CfA surveys [47, 82, 83] (see also the list of nearby projects given in Sec. 1.1).

The HST program led by Adam Riess [90, 99] dramatically enlarged the observed redshift range of SNe Ia. Thanks to the near-IR capabilities from space, the $z > 1$ domain was opened, allowing the study of SNe in the decelerated phase of the expansion, i.e. exploring the transition between acceleration and deceleration marked by the turn-around of the differential Hubble diagram in the bottom panel of Figure 3.

Progress at $z > 0.9$ is slower, mainly because it hinges on major access to near-IR observations with HST. The SN detection efficiency can be improved by targeting massive galaxy clusters, as demonstrated by [100]. Currently, a massive project to find very distant ($z > 1.5$) supernovae has started making use of two multi-cycle HST projects, which image several areas and galaxy clusters, over several years. Yet, it is unlikely that the number of $z > 1$ SNe Ia that can be used in the Hubble diagram will exceed ~ 100 with current instruments.

The cosmological results are summarized in Table 1.

The results are compatible and the strongest deviations come from the use

of the light curve fitters (and their assumptions on reddening; see Sec. 6.4). It should also be pointed out that the samples are not completely independent. The nearby supernova sample for almost all results presented in Tab. 1 are identical. The Union2 data set is the collection of all published SN Ia data suitable for cosmology.

6 Systematic uncertainties

6.1 Calibration

Precise distance estimates with Type Ia supernovae require very accurate relative photometry ($\Delta w \approx 2\Delta m$). While future surveys are likely to measure most (all) their SNe with a single, well calibrated system, current cosmological bounds are derived from a compilation of surveys. There is a worry for calibration offsets between the data sets, potentially resulting in a bias in the fitted cosmology. The SNLS team has been extremely active in refining the calibration of the CFHT MegaCam system and have reached sub-percent precision in their photometric calibration [101]. Unfortunately, significant calibration uncertainties remain for the near-IR HST system, including NICMOS nonlinearities. This amounts to a sizable contribution to the budget of systematic errors for the $z \gtrsim 1$ SNe Ia measured up to now [102]. Clearly, future SN Ia programs must integrate a robust calibration program into the survey design.

6.2 The UV-flux

Since high-z surveys are mostly confined to optical bands, the measured (red-shifted) fluxes originate at ultraviolet and blue wavelengths. For restframe wavelengths shorter than what corresponds to the B-band, several sources of concern

have been raised. The atmospheric cut-off and steeply falling instrument sensitivity has lead to significant difficulties in providing a good estimate of the intrinsic brightness in the U-band. About 5% of the SNIa flux is emitted at wavelengths shorter than the U-band, not at all accessible from the ground for $z = 0$. The wavelength region below $3000\,\text{Å}$ remains one of the least explored, in spite of the fact that it is rich in key information, e.g., about the underlying explosion physics. Furthermore, since the dimming by dust grains increases rapidly at shorter wavelengths, the uncertainty in host galaxy dust extinction properties and intrinsic color variations are major limitations for precise distance measurements.

Photometric studies with the *Swift* satellite [103, 104] and STIS spectroscopy with HST [105] have been used to test model predictions suggesting an increased dispersion in the UV, because of its larger sensitivity to progenitor composition [106–108]. These studies, as well as similar ones at $z \sim 0.5$ [109] do indeed find a scatter about twice as large in the UV compared to the optical.

It remains unclear what these effects mean for the use of SNIa as distance indicators.

6.3   Reddening and absorption

Accurate corrections for absorption of the SN light along the path from the source to the telescope are crucial for distance determinations. Interactions of light and dust grains may happen in the circumstellar material around the exploding star, in the interstellar medium of the host galaxy, in the intergalactic medium and in the Milky Way. Absorption in the Earth's atmosphere is corrected through the photometric calibration. The distribution and properties of dust grains in the Milky Way is known well enough to allow for correction accurate at the

sub-percent level. The other terms remain more problematic. The dust size-distribution is captured by the Galactic extinction law and is often described by the total-to-selective extinction ratio, R_V. For the Milky Way, an average value $R_V = 3.1$ has been found [76], with relatively small scatter around this value across the galaxy. The existence of significant amounts of intergalactic dust, $\Omega_{dust} \sim 10^{-6} - 10^{-5}$, has been inferred from estimates of the stellar density and metallicity as a function of redshift. After the evidence for cosmic acceleration was presented in 1998, several authors studied the possibility that the faintness of SNe Ia at high-z could instead be caused by "gray" interstellar dust in the inter-galactic medium [110–112]. An upper limit on the restframe B-band attenuation $A_B(z = 1) < 0.1$ on impact of dimming by dust in the intergalactic medium was derived by studies of quasar colors [113, 114].

More recently, Menard *et al.* [115] performed a cross-correlation study between colors of nearby and distant quasars and reported a statistical detection of dust reddening up to large scales around galaxies. From this result, they inferred the opacity of the universe. Their model-dependent estimate gives $A_B(z = 0.3) \approx$ 0.02 mag. This attenuation is partially compensated by the color-brightness correction. However, since the attenuation happens along the line of sight rather than at the redshift of the SN, the current light curve fitters cannot account for this effect in its totality as they correct for discrete redshifts of the host galaxy.

Considerably larger extinction by dust may occur in the interstellar medium of the host galaxy, especially for SN explosions close to the galaxy center. Multi-band photometry of SNe Ia has been used to constrain the wavelength dependence of the absorption. There is by now a large number of studies reporting measurements of $R_V \sim 2$ based on SN Ia colors, (e.g. [116–121]). Moreover, low-values

of R_V do also provide a smaller scatter in the Hubble diagram and thus a better fit in global parameter fitting of SNe Ia across a wide redshift range. This is somewhat puzzling and indicates that reddening by dust is not fully understood.

Multiple scattering of photons has been suggested as possible explanation to the "unexpected" reddening law. This could be the case in the presence of dust in the circumstellar environment of the SN Ia progenitor, as suggested by [122], who also provided an effective reddening law that gives good fits to the best measured/most reddened SNe Ia in the CSP low-z sample [49]. Spectroscopic evidence for circumstellar material around highly reddened SNe Ia has been found in e.g. [123].

At this point, the lack of understanding of the relative strengths and specific properties of the various effects contributing to the color-brightness relation of SNe Ia constitutes one of the biggest concerns, especially since a redshift dependence cannot be excluded.

6.4   Light curve fitters

Establishing the peak brightness of SNe Ia has to date been essential essential for their use in cosmology. A major progress over the past decade has been the much more systematic sampling of supernova observations. While the light curves of early supernovae had to be established from rather sparsely sampled data, the current and future surveys provide a much denser temporal coverage and the determination of the peak brightness is highly improved. However, light curve shape and reddening have to be established through fitting. Since color and shape are measured with respect to some reference set and may also include some additional priors, several light curve fitters have been proposed over the years.

Examples are the fitter developed by the SCP, SNMinuit, used the original light curve shapes in [124] based on low-z data, and improved in [71]. A "stretch" factor, s, was introduced to characterize the light curve shape perturbations with a simple scaling of the time axis within the, $t \cdot s$, and a corresponding brightness correction $\Delta M = \alpha \cdot (1 - s)$, i.e. broader light curves $s > 1$ corresponding to brighter intrinsic brightness, $\Delta M < 0$ (cf. Fig. 6). While s is fitted with points both in the rising and falling parts of the light curves, other shape estimates, like Δm_{15} [125], use only a limited region after maximum. The two major LC fitters used today are SALT2 [118] and MLCS2k2 [126], the second generations of SALT [127] and MLCS [128]. The major differences between the two reside in the reference spectral templates in the blue and UV regions and in the interpretation of reddening. While the MLCS approach is to obtain the reference samples from the low-z SNe, SALT combines data from both high and low redshift. In consequence, the MLCS "training" may be biased by the difficulties to obtain high quality data in the UV, as explained in section 6.2, whereas SALT may lack the ability to detect intrinsic changes with redshift and makes use of faint data. Another key difference involves the treatment of color-brightness relation. MLCS assumes that SN Ia reddening is caused by dust, thus negative color corrections are not used. In contrast, SALT combines all possible contributions into a single function relating the intensity as a function of wavelength, and both positive as well as negative corrections are allowed, i.e. a negative color excess implies increased brightness and reddening corresponds to dimming of light. An example of MLCS2k2 and SALT2 fits of the SNLS supernova 04D2gp ($z = 0.732$) is shown in Figure 9. Although both fits give good χ^2, SALT2 finds the SNe to be moderately blue, while MLCS2k2 puts it at small (but positive) extinction. Thus,

the derived distance modulus for this particular SN differs by 0.1 mag [98]. More recently, two other fitters have been developed SiFTO [129], so far only used by the SNLS collaboration, and SNooPy [64] by CSP that, unlike other fitters, can also be used to build near-IR light curves.

6.5   Selection bias

Varying selection efficiency is an inherent difficulty in a technique involving comparisons of brightness of objects at different redshifts. In particular, cosmological estimates using multiple surveys need to model (most often through Monte Carlo simulations) the fraction of the SN Ia luminosity function sampled by the detection requirements of each instrument. At high-z, the "bottle-neck" is the spectroscopic identification, which is only practically obtainable for $i < 25$ mag in 8-10 meter class telescopes. This naturally leads to a redshift dependent selection bias in magnitude and color, e.g., for the 3-year SNLS sample [97], as shown in Figure 10. Perrett *et al.* [130] examine these selection effects in detail, and the related corrections. A problem associated with these corrections is our lack of precise understanding of potential drifts in either reddening properties (Sec. 6.3) or intrinsic SN Ia luminosity, to be discussed further in Sec. 6.8. An ambitious space mission equipped with a multi-band imager and a sensitive spectrograph could potentially resolve this difficulty (see Sec. 8).

6.6   Gravitational lensing

In Section 2.1 we derived the expression for the luminosity distance used to measure cosmological parameters assuming that the universe is homogeneous and isotropic. Although there is ample empirical evidence that this is a good

approximation at the largest scales, e.g., from the cosmic microwave background, it is clear that inhomogeneities exist at smaller scales. Thus, foreground galaxy halos and clusters of galaxies act as gravitational lenses and introduce a "scatter" in the observed SN Ia flux that increases with redshift [131–133]. Since the number of photons is conserved under lensing (some objects get magnified and others de-magnified), the luminosity distance averaged over a large number of SNe Ia is expected to converge towards Eq. (10). However, for small number statistics or if the sample is magnitude limited, gravitational lensing could be a source of selection bias. This was first investigated in [134] for the HST GOODS sample [99], where the redshifts of the foreground galaxies are well measured and their masses can be estimated through their luminosities and the effect of lensing of individual SN can be evaluated. More recently, Jönsson *et al.* [135] have studied the weak lensing perturbations in the SNLS 3-year data (Figure 11). The distribution of lensing magnifications of SNe Ia as a function of redshift matches the expectations and no significant bias has been detected in the current high-z sample.

6.7 Peculiar velocities

Local matter inhomogeneities are also important for precision cosmology with SNe Ia. Local density perturbations induce peculiar velocities in galaxies of about 300 km s^{-1}. In addition, the exploding star could have a comparable internal motion within the host galaxy. Since these velocity components cannot be disentangled from the cosmological redshift, an extra source of uncertainty needs to be considered, $\sigma_\mu \approx \frac{v}{c} \cdot \frac{5}{\ln(10)} \left[\frac{1+z}{z(1+z/2)} \right]$, which exceeds the error from intrinsic brightness $\sigma_\mu \approx 0.1$ mag for $z < 0.015$. The concern, however, is not

the addition of an added "random" error, but rather the possibility of an effect that does not average out with statistics. In particular, our own motion and the correlated peculiar velocities of the SN Ia host galaxies at low-z could have a non-negligible effect on the derived cosmological parameters. Several authors have studied these effects, concluding that inclusion of SNe Ia down to $z = 0.02$ may result in a systematic uncertainty of about $\Delta w \lesssim 0.01$ [136].

6.8   Brightness evolution

The brightness distribution of SNe Ia has been shown to depend on the host galaxy environment. E.g. Hamuy *et al.* [137] noticed that the average B and V-band light curve width differs between galaxy types. It is now an established fact that elliptical galaxies host a larger fraction of narrower, low "stretch", supernovae. Furthermore, recent studies of nearby supernovae [138]; SNLS supernovae [139] and SDSS SNe [140] suggest possible evidence for varying supernova properties with host galaxy not entirely corrected by the standard width-color-brightness relations. In particular, it has been argued that splitting the sample according to host-galaxy mass and allowing the peak absolute magnitudes of the two samples to differ improves the residuals in a statistically significant manner. The evidence suggests that large stellar mass galaxies host the brightest SNe Ia ($\Delta M \sim 0.075$ mag), after light curve shape corrections. Given the time evolution of metallicity and stellar mass of galaxies, the possibility of a drift in the brightness of the "standard candle" with redshift remains a source of concern for precision cosmology.

6.9 The "averaging" uncertainty

After the discovery of dark energy several authors [141–145] raised doubts about the theoretical foundations leading to Eq. (14). In particular, it has been claimed that the average expansion in a locally inhomogeneous universe behaves differently than expected in Friedmann-Lemaitre models based on the large scale *average* energy density. The reason being the non-linearity of the Einstein equations: spatial averaging and solving the Einstein equations do not commute [146]. This is sometimes referred to as the "back-reaction" problem. Although the issue is generally accepted, arguments have been put forward for why the effect is too small to explain "cosmic acceleration" without dark energy. In a matter-dominated universe the local dynamics should be (almost) Newtonian, as long as potential perturbations and peculiar velocities are non-relativistic. Since Newtonian gravity is linear, averaging and evolution do commute in the Newtonian limit and should commute to a good approximation in general relativity [147,148]. Any relativistic corrections should be much to small to mimic effective acceleration. Since it is notoriously difficult to estimate the size of the effects from non-linear back-reaction in general relativity, it remains unclear at this point whether this presents a limitation for precision tests of w.

7 Recent developments

7.1 Expanding the wavelength window

The use of Type Ia supernovae helped establish a major milestone in precision cosmology, especially the discovery of dark energy. However, further progress in the field is limited by our ability to resolve the systematic uncertainties outlined in

Section 6. Some outstanding issues involve understanding the progenitor system leading to Type Ia supernovae and the properties of dust extinction affecting SN Ia. A natural path that has been followed for this purpose is to expand the studied wavelength window, especially for nearby SNe. Furthermore, theoretical arguments have been put forward suggesting that the dispersion of intrinsic SNIa peak magnitudes should have a minimum around 1.6μm [59].

7.1.1   THE NEAR-IR   The Earth's atmosphere severely limits the feasibility of ground based observations in the near-IR. Vibrational bands of H_20 and CO_2 block the incoming radiation beyond 1 μm, leaving a few observational windows in the near-IR: J, H and K-bands, centered at $1.2, 1.6$ and 2.2 μm, respectively. To make matters worse, significant thermal atmospheric emission (mostly from multiple narrow OH-lines) reduces the obtainable signal-to-noise ratio. This is particularly challenging since the fractional flux in the near-IR is small for SNIa: 2, 1 and 0.5 % for J, H, K [14]. In spite of these difficulties, significant efforts have been devoted recently to studies of supernovae in the near-IR. A non-standard extinction law has been measured with great accuracy for a number of highly reddened SNIa with high S/N near-IR data [49, 117, 119, 121, 149]. Moreover, statistical tests on $z < 0.05$ SNIa in [49, 150–152] offer observational support for the claim in [59] of a somewhat narrower intrinsic scatter in the near-IR. However, this benefit may only be exploited at high-redshift with space based observations, e.g. the James Webb Space Telescope. Because of the paucity of data in near-IR, and the very narrow redshift range studied, it is yet unclear if problems with K-corrections may arise, i.e., varying spectral features moving in and out of the filter pass-band as the redshift increases. An interesting development taking place in recent years, and more easily accessible than the restframe NIR,

is building a Hubble diagram in restframe I-band, i.e., at about 8000 Å [153,154].

In particular, Freedman *et al.* [155] use a sample of 56 SNIa; 21 nearby, and 35 in

the redshift range $0.1 < z < 0.7$, and find limits on w which are consistent with

the results at shorter wavelengths.

7.2 Spectral indicators as secondary calibrators

Thanks to the availability of large spectroscopic sets of SNIa, both nearby and at

cosmological distances, data mining efforts have been conducted trying to identify

spectral indicators capable of refining the intrinsic dispersion of the "standard

candle", e.g., [33, 34, 109, 156–168]. Although some of these findings could have

a profound impact in our understanding of the physics behind SNIa explosions

and optimize their use in cosmology, the statistical evidence and interpretation

of the correlations needs further assessment.

8 Supernova cosmology for the next decade

The goal of the next supernova cosmology surveys must be to reach a level of

accuracy promising to meaningfully constrain a time-dependent $w(t)$. From the

descriptions of the systematics of the supernova cosmology, it is clear that a strict

control of the surveys is required. This has led to the concentration on singular

telescopes and their calibration for the searches and the photometry. Finding

potential further correlations in the SN Ia observations can further sharpen the

acuity of SNe Ia for cosmological distances and will also give hints on the super-

nova physics. Another improvement would be to explore the small luminosity

scatter of SNe Ia in the near-infrared. Building a well-sampled Hubble diagram

at near-infrared wavelengths would reduced the uncertainties on the reddening

corrections as well.

Several programs aiming at discovering thousands of SNe Ia up to $z = 1$ are in the process of starting up. The "rolling search" technique, where CCD cameras with very large field of view are used to revisit sky pointings with cadences of a few days, has been proved very successful, e.g., by SNLS using the 1-square-degree at the 3.6m CFHT in Hawaii. New SNe are found while multi-band light curves are built for transients discovered in earlier epochs. With the imminent start of operations of the Dark Energy Survey (DES) on the CTIO 4m (Chile) using a new 3 square degree mosaic CCD camera, about 3000 SNe Ia are expected within 5 years. The redshift range will overlap with the existing samples from SDSS, SNLS and ESSENCE.

A fully developed Pan-STARRS with four 1.8m telescopes observing simultaneously will have the capability to scan the entire sky within just a week. With the 3-square-degree CCD array on each unit and a pixel size of 0.3 arc-seconds, a large number of SNe Ia can be found across a wide redshift range. The first prototype unit, Pan-STARRS1, is already collecting data and several supernova discoveries have been reported.

The 8-meter telescope foreseen in the LSST project, carrying a 9-square-degree camera and performing repeat all sky imaging in five optical bands will propel the art of finding supernovae to a whole new dimension. With an expected yearly yield of 250000 SNe Ia, with light curves sampled every five days, low- and high-z supernovae will be found with the same instrument and calibrated to about 1% photometric precision.

The limitation of this project lies also in the big numbers: it is impossible to get spectroscopic identification for more than a small subset of supernovae. The

redshift determination most likely will be done through photometric redshifts of the host galaxies. Thus, the success of the LSST SN Ia program for cosmology depends on the accuracy of the photometric identification and control of systematic uncertainties related to e.g., a possible evolution of the standard candle and brightness-color corrections, as discussed in Sec.6.

First proposed in 1999, the SuperNova Acceleration Probe (SNAP) was for a long time the leading concept for a dedicated satellite mission aiming at the study of the properties of dark energy with SNIa. Several competing designs have been proposed in the mean time, focusing on one or several cosmological probes: Type Ia supernovae, weak lensing measurements and baryon acoustic oscillations. At present, two missions are being considered: the European-led EUCLID satellite and a US-proposed WFIRST. ESA's EUCLID is mainly focusing on baryonic acoustic oscillations and weak lensing and the current specifications include only a broad optical ("visible") and three near-infrared filters, which is arguably non-optimal for precision studies of SN Ia over a wide range of redshifts. The WFIRST mission concept includes SN Ia (as well as baryonic acoustic oscillations and weak lensing) and a 1.5-meter class telescope has been proposed as a reference. Although a space mission cannot compete with LSST in statistics of SNe Ia, it is likely to collect a much better studied sample of SN Ia, including near-IR observations and possibly spectrophotometry, thereby having a better control of systematic uncertainties, the ultimate limitation in studying the properties of dark energy with SNIa.

Figure 12 shows the projected sensitivity of WFIRST in the (w_0, w_a) parameter space compared with the current constraints from the Union2 sample in Amanullah *et al.* (2010) [69]. The shaded "petals" in the figure show classes

of "quintessence" models, i.e., where a scalar field dominates the current energy density of the universe [4]. One such case is the pseudo Nambu-Goldstone boson (PNGB) [169], e.g., an axion with a Hubble scale (H_0^{-1}) Compton wavelength, i.e., a mass $m \sim 10^{-33}$ eV. Predictions from String Theory inspired scalar field potentials in gravitational theories with extra dimensions (SUGRA) and the braneworld model by Dvali and Turner [170] are also shown for reference. Clearly, *any* deviation from Λ would be dramatic breakthrough in fundamental physics. Observational cosmology, and distance estimates with SNe Ia in particular, will continue to contribute to the full picture of high-energy and particle physics.

LITERATURE CITED

1. Kamionkowski M, Kosowsky A, Annual Review of Nuclear and Particle Science 49:77 (1999), arXiv:astro-ph/9904108.

2. Hu W, Dodelson S, ARA&A, 40:171 (2002), arXiv:astro-ph/0110414.

3. Samtleben D, Staggs S, Winstein B, Annual Review of Nuclear and Particle Science 57:245 (2007), 0803.0834.

4. Caldwell RR, Linder EV, Physical Review Letters 95:141301 (2005),

arXiv:astro-ph/0505494.

5. Copeland EJ, Sami M, Tsujikawa S, International Journal of Modern Physics D 15:1753 (2006), arXiv:hep-th/0603057.

6. Kowal CT, AJ,73:1021 (1968).

7. Branch D, Tammann GA, ARA&A, 30:359 (1992).

8. Branch D, ARA&A, 36:17 (1998), arXiv:astro-ph/9801065.

9. Nugent P, Sullivan M, Ellis R, Gal-Yam A, Leonard DC, et al., ApJ,645:841 (2006), arXiv:astro-ph/0603535.

10. Leibundgut B, ARA&A, 39:67 (2001).

11. Leibundgut B, General Relativity and Gravitation 40:221 (2008), 0802.4154.

12. Frieman JA, Turner MS, Huterer D, ARA&A, 46:385 (2008), 0803.0982.

13. Caldwell RR, Kamionkowski M, Annual Review of Nuclear and Particle Science 59:397 (2009), 0903.0866.

14. Howell DA, ArXiv e-prints (2010), 1011.0441.

15. Riess AG, Filippenko AV, Challis P, Clocchiatti A, Diercks A, et al., AJ,116:1009 (1998), arXiv:astro-ph/9805201.

16. Perlmutter S, Aldering G, Goldhaber G, Knop RA, Nugent P, et al., ApJ,517:565 (1999), arXiv:astro-ph/9812133.

17. Weinberg S, Physical Review Letters 59:2607 (1987).

18. Vilenkin A, Physical Review Letters 74:846 (1995), arXiv:gr-qc/9406010.

19. Loeb A, J. Cosmology Astropart. Phys.,5:9 (2006), arXiv:astro-ph/0604242.

20. Report No., , 2006 (unpublished), arXiv:astro-ph/0610906.

21. Albrecht A, Bernstein G, Cahn R, Freedman WL, Hewitt J, et al., ArXiv Astrophysics e-prints (2006), arXiv:astro-ph/0609591.

22. Freedman WL, Madore BF, ARA&A, 48:673 (2010), 1004.1856.

23. Riess AG, PASP,112:1284 (2000), arXiv:astro-ph/0005229.

24. Perlmutter S, Physics Today 56:040000 (2003).

25. Perlmutter S, Schmidt BP, Measuring Cosmology with Supernovaein *Supernovae and Gamma-Ray Bursters*, , volume 598 of *Lecture Notes in Physics, Berlin Springer Verlag*, pp. 195–217, 2003, arXiv:astro-ph/0303428.

26. Baade W, Zwicky F, Physical Review 46:76 (1934).

27. Lundmark K, MNRAS,85:865 (1925).

28. Minkowski R, PASP,53:224 (1941).

29. Minkowski R, ARA&A, 2:247 (1964).

30. Filippenko AV, ARA&A, 35:309 (1997).

31. Zwicky F, Supernovaein *Stellar Structure - Stars and Stellar Systems*, , pp. 367–+, 1965.

32. Branch D, Dang LC, Baron E, PASP,121:238 (2009), 0902.0745.

33. Blondin S, Dessart L, Leibundgut B, Branch D, Höflich P, et al., AJ,131:1648 (2006), arXiv:astro-ph/0510089.

34. Benetti S, Cappellaro E, Mazzali PA, Turatto M, Altavilla G, et al., ApJ,623:1011 (2005), arXiv:astro-ph/0411059.

35. Nordin J, Östman L, Goobar A, Amanullah R, Nichol RC, et al., A&A, 526:A119+ (2011), 1011.6227.

36. Hamuy M, Phillips MM, Suntzeff NB, Maza J, González LE, et al., Nature, 424:651 (2003), arXiv:astro-ph/0306270.

37. Howell DA, Sullivan M, Nugent PE, Ellis RS, Conley AJ, et al., Nature, 443:308 (2006), arXiv:astro-ph/0609616.

38. Hicken M, Garnavich PM, Prieto JL, Blondin S, DePoy DL, et al., ApJ,669:L17 (2007), 0709.1501.

39. Silverman JM, Ganeshalingam M, Li W, Filippenko AV, Miller AA, Poznanski D, MNRAS,410:585 (2011), 1003.2417.

40. Li W, Filippenko AV, Gates E, Chornock R, Gal-Yam A, et al., PASP,113:1178 (2001), arXiv:astro-ph/0107318.

41. Li W, Filippenko AV, Chornock R, Berger E, Berlind P, et al., PASP,115:453 (2003), arXiv:astro-ph/0301428.

42. Phillips MM, Li W, Frieman JA, Blinnikov SI, DePoy D, et al., PASP,119:360 (2007), arXiv:astro-ph/0611295.

43. Foley RJ, Chornock R, Filippenko AV, Ganeshalingam M, Kirshner RP, et al., AJ,138:376 (2009), 0902.2794.

44. Valenti S, Pastorello A, Cappellaro E, Benetti S, Mazzali PA, et al., Nature, 459:674 (2009), 0901.2074.

45. Li W, Leaman J, Chornock R, Filippenko AV, Poznanski D, et al., ArXiv e-prints (2010), 1006.4612.

46. Leibundgut B, A&A Rev.10:179 (2000), arXiv:astro-ph/0003326.

47. Hicken M, Challis P, Jha S, Kirshner RP, Matheson T, et al., ApJ,700:331 (2009), 0901.4787.

48. Ganeshalingam M, Li W, Filippenko AV, Anderson C, Foster G, et al., ApJS,190:418 (2010).

49. Folatelli G, Phillips MM, Burns CR, Contreras C, Hamuy M, et al., AJ,139:120 (2010), 0910.3317.

50. Rau A, Kulkarni SR, Law NM, Bloom JS, Ciardi D, et al., PASP,121:1334 (2009), 0906.5355.

51. Woosley S, Janka T, Nature Physics 1:147 (2005), arXiv:astro-ph/0601261.

52. Hillebrandt W, Niemeyer JC, ARA&A, 38:191 (2000), arXiv:astro-

ph/0006305.

53. Röpke FK, Hillebrandt W, Schmidt W, Niemeyer JC, Blinnikov SI, Mazzali PA, ApJ,668:1132 (2007), 0707.1024.

54. Pakmor R, Kromer M, Röpke FK, Sim SA, Ruiter AJ, Hillebrandt W, Nature, 463:61 (2010), 0911.0926.

55. Fink M, Hillebrandt W, Röpke FK, A&A, 476:1133 (2007), 0710.5486.

56. Fink M, Röpke FK, Hillebrandt W, Seitenzahl IR, Sim SA, Kromer M, A&A, 514:A53+ (2010), 1002.2173.

57. Diehl R, Timmes FX, PASP,110:637 (1998).

58. Kromer M, Sim SA, MNRAS,398:1809 (2009), 0906.3152.

59. Kasen D, ApJ,649:939 (2006), arXiv:astro-ph/0606449.

60. Kasen D, Röpke FK, Woosley SE, Nature, 460:869 (2009), 0907.0708.

61. Stritzinger M, Leibundgut B, Walch S, Contardo G, A&A, 450:241 (2006), arXiv:astro-ph/0506415.

62. Li W, Chornock R, Leaman J, Filippenko AV, Poznanski D, et al., ArXiv e-prints (2010), 1006.4613.

63. Dilday B, Smith M, Bassett B, Becker A, Bender R, et al., ApJ,713:1026 (2010), 1001.4995.

64. Burns CR, Stritzinger M, Phillips MM, Kattner S, Persson SE, et al., AJ,141:19 (2011), 1010.4040.

65. Dahlen T, Strolger L, Riess AG, ApJ,681:462 (2008), 0803.1130.

66. Dahlen T, Strolger L, Riess AG, Mobasher B, Chary R, et al., ApJ,613:189 (2004), arXiv:astro-ph/0406547.

67. Mannucci F, Della Valle M, Panagia N, MNRAS,377:1229 (2007), arXiv:astro-ph/0702355.

68. Bergström L, Goobar A, *Cosmology and particle astrophysics., Berlin, Germany: Springer (2004)* .

69. Amanullah R, Lidman C, Rubin D, Aldering G, Astier P, et al., ApJ,716:712 (2010), 1004.1711.

70. Leibundgut B, Schommer R, Phillips M, Riess A, Schmidt B, et al., ApJ,466:L21+ (1996), arXiv:astro-ph/9605134.

71. Goldhaber G, Groom DE, Kim A, Aldering G, Astier P, et al., ApJ,558:359 (2001), arXiv:astro-ph/0104382.

72. Blondin S, Davis TM, Krisciunas K, Schmidt BP, Sollerman J, et al., ApJ,682:724 (2008), 0804.3595.

73. Amanullah R, Stanishev V, Goobar A, Schahmaneche K, Astier P, et al., A&A, 486:375 (2008), 0711.1375.

74. Stanishev V, Goobar A, Benetti S, Kotak R, Pignata G, et al., A&A, 469:645 (2007), 0704.1244.

75. Lidman C, Howell DA, Folatelli G, Garavini G, Nobili S, et al., A&A, 430:843 (2005), arXiv:astro-ph/0410506.

76. Cardelli JA, Clayton GC, Mathis JS, ApJ,345:245 (1989).

77. Kim A, Goobar A, Perlmutter S, PASP,108:190 (1996), arXiv:astro-ph/9505024.

78. Freedman WL, Madore BF, Gibson BK, Ferrarese L, Kelson DD, et al., ApJ,553:47 (2001), arXiv:astro-ph/0012376.

79. Riess AG, Macri L, Casertano S, Sosey M, Lampeitl H, et al., ApJ,699:539 (2009), 0905.0695.

80. Goobar A, Perlmutter S, ApJ,450:14 (1995), arXiv:astro-ph/9505022.

81. Hamuy M, Phillips MM, Suntzeff NB, Schommer RA, Maza J, Aviles R,

AJ,112:2398 (1996), arXiv:astro-ph/9609062.

82. Riess AG, Kirshner RP, Schmidt BP, Jha S, Challis P, et al., AJ,117:707 (1999), arXiv:astro-ph/9810291.

83. Jha S, Kirshner RP, Challis P, Garnavich PM, Matheson T, et al., AJ,131:527 (2006), arXiv:astro-ph/0509234.

84. Kowalski M, Rubin D, Aldering G, Agostinho RJ, Amadon A, et al., ApJ,686:749 (2008), 0804.4142.

85. Tonry JL, Schmidt BP, Barris B, Candia P, Challis P, et al., ApJ,594:1 (2003), arXiv:astro-ph/0305008.

86. Knop RA, Aldering G, Amanullah R, Astier P, Blanc G, et al., ApJ,598:102 (2003), arXiv:astro-ph/0309368.

87. Krisciunas K, Garnavich PM, Challis P, Prieto JL, Riess AG, et al., AJ,130:2453 (2005), arXiv:astro-ph/0508681.

88. Barris BJ, Tonry JL, Blondin S, Challis P, Chornock R, et al., ApJ,602:571 (2004), arXiv:astro-ph/0310843.

89. Astier P, Guy J, Regnault N, Pain R, Aubourg E, et al., A&A, 447:31 (2006), arXiv:astro-ph/0510447.

90. Riess AG, Strolger L, Casertano S, Ferguson HC, Mobasher B, et al., ApJ,659:98 (2007), arXiv:astro-ph/0611572.

91. Miknaitis G, Pignata G, Rest A, Wood-Vasey WM, Blondin S, et al., ApJ,666:674 (2007), arXiv:astro-ph/0701043.

92. Holtzman JA, Marriner J, Kessler R, Sako M, Dilday B, et al., AJ,136:2306 (2008), 0908.4277.

93. Percival WJ, Reid BA, Eisenstein DJ, Bahcall NA, Budavari T, et al., MN-RAS,401:2148 (2010), 0907.1660.

94. Komatsu E, Smith KM, Dunkley J, Bennett CL, Gold B, et al., ArXiv e-prints (2010), 1001.4538.

95. Eisenstein DJ, Zehavi I, Hogg DW, Scoccimarro R, Blanton MR, et al., ApJ,633:560 (2005), arXiv:astro-ph/0501171.

96. Wood-Vasey WM, Miknaitis G, Stubbs CW, Jha S, Riess AG, et al., ApJ,666:694 (2007), arXiv:astro-ph/0701041.

97. Guy J, Sullivan M, Conley A, Regnault N, Astier P, et al., A&A, 523:A7+ (2010), 1010.4743.

98. Kessler R, Becker AC, Cinabro D, Vanderplas J, Frieman JA, et al., ApJS,185:32 (2009), 0908.4274.

99. Riess AG, Strolger L, Tonry J, Casertano S, Ferguson HC, et al., ApJ,607:665 (2004), arXiv:astro-ph/0402512.

100. Dawson KS, Aldering G, Amanullah R, Barbary K, Barrientos LF, et al., AJ,138:1271 (2009), 0908.3928.

101. Regnault N, Conley A, Guy J, Sullivan M, Cuillandre J, et al., A&A, 506:999 (2009), 0908.3808.

102. Conley A, Guy J, Sullivan M, Regnault N, Astier P, et al., ApJS,192:1 (2011).

103. Brown PJ, Roming PWA, Milne P, Bufano F, Ciardullo R, et al., ApJ,721:1608 (2010), 1007.4842.

104. Milne PA, Brown PJ, Roming PWA, Holland ST, Immler S, et al., ApJ,721:1627 (2010), 1007.5279.

105. Cooke J, Ellis RS, Sullivan M, Nugent P, Howell DA, et al., ArXiv e-prints (2010), 1010.2211.

106. Lentz EJ, Baron E, Branch D, Hauschildt PH, Nugent PE, ApJ,530:966

(2000), arXiv:astro-ph/9906016.

107. Höflich P, Nomoto K, Umeda H, Wheeler JC, ApJ,528:590 (2000), arXiv:astro-ph/9908226.

108. Sauer DN, Mazzali PA, Blondin S, Stehle M, Benetti S, et al., MN-RAS,391:1605 (2008), 0803.0871.

109. Ellis RS, Sullivan M, Nugent PE, Howell DA, Gal-Yam A, et al., ApJ,674:51 (2008), 0710.3896.

110. Aguirre AN, ApJ,512:L19 (1999), arXiv:astro-ph/9811316.

111. Aguirre A, ApJ,525:583 (1999), arXiv:astro-ph/9904319.

112. Goobar A, Bergström L, Mörtsell E, A&A, 384:1 (2002), arXiv:astro-ph/0201012.

113. Mörtsell E, Goobar A, J. Cosmology Astropart. Phys.,9:9 (2003), arXiv:astro-ph/0308046.

114. Östman L, Mörtsell E, J. Cosmology Astropart. Phys.,2:5 (2005), arXiv:astro-ph/0410501.

115. Ménard B, Scranton R, Fukugita M, Richards G, MNRAS,405:1025 (2010), 0902.4240.

116. Krisciunas K, Prieto JL, Garnavich PM, Riley J, Rest A, et al., AJ,131:1639 (2006), arXiv:astro-ph/0511162.

117. Elias-Rosa N, Benetti S, Cappellaro E, Turatto M, Mazzali PA, et al., MN-RAS,369:1880 (2006), arXiv:astro-ph/0603316.

118. Guy J, Astier P, Baumont S, Hardin D, Pain R, et al., A&A, 466:11 (2007), arXiv:astro-ph/0701828.

119. Krisciunas K, Garnavich PM, Stanishev V, Suntzeff NB, Prieto JL, et al., AJ,133:58 (2007), arXiv:astro-ph/0609268.

120. Nobili S, Goobar A, A&A, 487:19 (2008), 0712.1155.

121. Elias-Rosa N, Benetti S, Turatto M, Cappellaro E, Valenti S, et al., MN-RAS,384:107 (2008), 0710.4503.

122. Goobar A, ApJ,686:L103 (2008), 0809.1094.

123. Patat F, Chandra P, Chevalier R, Justham S, Podsiadlowski P, et al., Science 317:924 (2007), 0707.2793.

124. Leibundgut B, *Light curves of supernovae type, I.*, PhD thesis, PhD thesis. Univ. Basel.137 pp. , (1988), 1988.

125. Phillips MM, Lira P, Suntzeff NB, Schommer RA, Hamuy M, Maza J, AJ,118:1766 (1999), arXiv:astro-ph/9907052.

126. Jha S, Riess AG, Kirshner RP, ApJ,659:122 (2007), arXiv:astro-ph/0612666.

127. Guy J, Astier P, Nobili S, Regnault N, Pain R, A&A, 443:781 (2005), arXiv:astro-ph/0506583.

128. Riess AG, Press WH, Kirshner RP, ApJ,473:88 (1996), arXiv:astro-ph/9604143.

129. Conley A, Sullivan M, Hsiao EY, Guy J, Astier P, et al., ApJ,681:482 (2008), 0803.3441.

130. Perrett K, Balam D, Sullivan M, Pritchet C, Conley A, et al., AJ,140:518 (2010), 1006.2254.

131. Bergström L, Goliath M, Goobar A, Mörtsell E, A&A, 358:13 (2000), arXiv:astro-ph/9912194.

132. Holz DE, Linder EV, ApJ,631:678 (2005), arXiv:astro-ph/0412173.

133. Mörtsell E, Gunnarsson C, Goobar A, ApJ,561:106 (2001), arXiv:astro-ph/0105355.

134. Jönsson J, Dahlén T, Goobar A, Gunnarsson C, Mörtsell E, Lee K,

ApJ,639:991 (2006), arXiv:astro-ph/0506765.

135. Jönsson J, Sullivan M, Hook I, Basa S, Carlberg R, et al., MNRAS,405:535 (2010), 1002.1374.

136. Davis TM, Hui L, Frieman JA, Haugbølle T, Kessler R, et al., ArXiv e-prints (2010), 1012.2912.

137. Hamuy M, Phillips MM, Suntzeff NB, Schommer RA, Maza J, Aviles R, AJ,112:2391 (1996), arXiv:astro-ph/9609059.

138. Kelly PL, Hicken M, Burke DL, Mandel KS, Kirshner RP, ApJ,715:743 (2010), 0912.0929.

139. Sullivan M, Conley A, Howell DA, Neill JD, Astier P, et al., MNRAS,406:782 (2010), 1003.5119.

140. Lampeitl H, Smith M, Nichol RC, Bassett B, Cinabro D, et al., ApJ,722:566 (2010), 1005.4687.

141. Buchert T, Kerscher M, Sicka C, Phys. Rev. D62:043525 (2000), arXiv:astro-ph/9912347.

142. Célérier M, ArXiv Astrophysics e-prints (2007), arXiv:astro-ph/0702416.

143. Wiltshire DL, Phys. Rev. D80:123512 (2009), 0909.0749.

144. Rasanen S, ArXiv e-prints (2010), 1012.0784.

145. Kolb EW, Marra V, Matarrese S, General Relativity and Gravitation 42:1399 (2010), 0901.4566.

146. Ellis GFR, Relativistic cosmology - Its nature, aims and problemsin *General Relativity and Gravitation Conference*, , pp. 215–288, 1984.

147. Ishibashi A, Wald RM, Classical and Quantum Gravity 23:235 (2006), arXiv:gr-qc/0509108.

148. Flanagan ÉÉ, Phys. Rev. D71:103521 (2005), arXiv:hep-th/0503202.

149. Wang X, Li W, Filippenko AV, Krisciunas K, Suntzeff NB, et al., ApJ,675:626 (2008), 0708.0140.

150. Wood-Vasey WM, Friedman AS, Bloom JS, Hicken M, Modjaz M, et al., ApJ,689:377 (2008), 0711.2068.

151. Mandel KS, Wood-Vasey WM, Friedman AS, Kirshner RP, ApJ,704:629 (2009), 0908.0536.

152. Mandel KS, Narayan G, Kirshner RP, ArXiv e-prints (2010), 1011.5910.

153. Nobili S, Amanullah R, Garavini G, Goobar A, Lidman C, et al., A&A, 437:789 (2005), arXiv:astro-ph/0504139.

154. Nobili S, Fadeyev V, Aldering G, Amanullah R, Barbary K, et al., ApJ,700:1415 (2009), 0906.4318.

155. Freedman WL, Burns CR, Phillips MM, Wyatt P, Persson SE, et al., ApJ,704:1036 (2009), 0907.4524.

156. Hook IM, Howell DA, Aldering G, Amanullah R, Burns MS, et al., AJ,130:2788 (2005), arXiv:astro-ph/0509041.

157. Branch D, Dang LC, Hall N, Ketchum W, Melakayil M, et al., PASP,118:560 (2006), arXiv:astro-ph/0601048.

158. Garavini G, Folatelli G, Nobili S, Aldering G, Amanullah R, et al., A&A, 470:411 (2007), arXiv:astro-ph/0703629.

159. Foley RJ, Filippenko AV, Aguilera C, Becker AC, Blondin S, et al., ApJ,684:68 (2008), 0710.2338.

160. Bronder TJ, Hook IM, Astier P, Balam D, Balland C, et al., A&A, 477:717 (2008), 0709.0859.

161. Sullivan M, Ellis RS, Howell DA, Riess A, Nugent PE, Gal-Yam A, ApJ,693:L76 (2009), 0901.2476.

162. Bailey S, Aldering G, Antilogus P, Aragon C, Baltay C, et al., A&A, 500:L17 (2009), 0905.0340.

163. Wang X, Filippenko AV, Ganeshalingam M, Li W, Silverman JM, et al., ApJ,699:L139 (2009), 0906.1616.

164. Walker ES, Hook IM, Sullivan M, Howell DA, Astier P, et al., MNRAS,:1811 (2010), 1008.2308.

165. Foley RJ, Kasen D, ArXiv e-prints (2010), 1011.4517.

166. Nordin J, Ostman L, Goobar A, Amanullah R, Nichol RC, et al., ArXiv e-prints (2010), 1011.6227.

167. Nordin J, Ostman L, Goobar A, Balland C, Lampeitl H, et al., ArXiv e-prints (2010), 1012.4430.

168. Blondin S, Mandel KS, Kirshner RP, A&A, 526:A81+ (2011), 1012.0005.

169. Frieman JA, Hill CT, Stebbins A, Waga I, Physical Review Letters 75:2077 (1995), arXiv:astro-ph/9505060.

170. Dvali G, Turner MS, ArXiv Astrophysics e-prints (2003), arXiv:astro-ph/0301510.
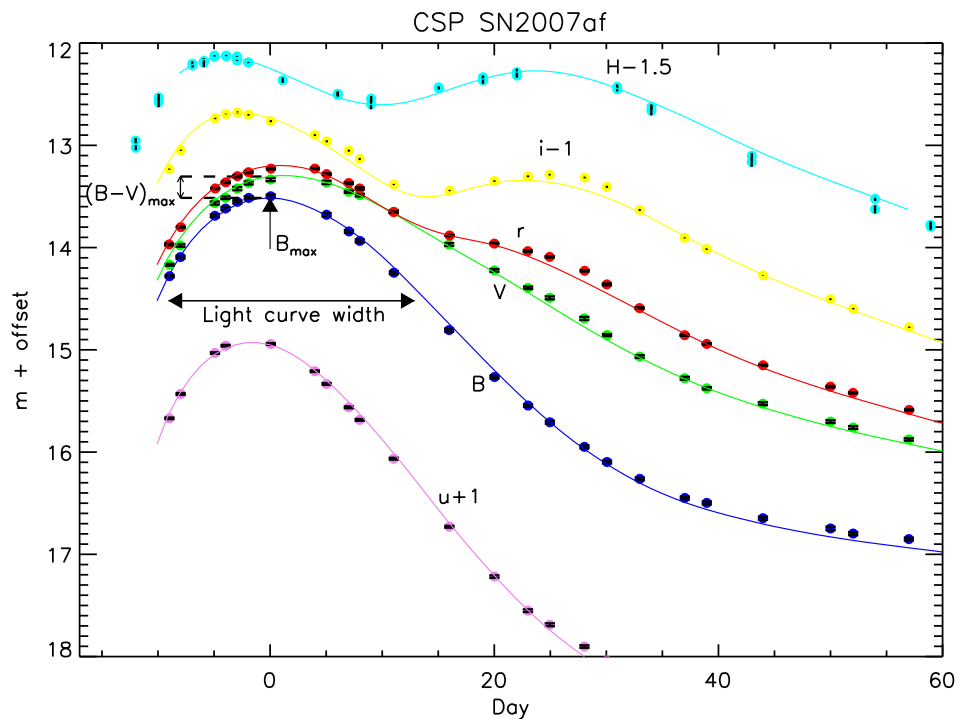
Figure 1: Optical and near-infrared light curves of the nearby SN 2007af obtained by the Carnegie Supernova Project (Stritzinger *et al.* in prep.). The light curves trace the brightness evolution in six different wavelength passbands ranging from ∼3500Å (u) to 1.6 μm (H). For clarity the individual filter light curves have been offset by the amounts indicated. Light curve fits [64] are shown and the key fit parameters (time and magnitude at maximum, the width of the light curve and a typical color "B-V") are marked. The development of the second peak with increasing wavelengths is very prominent. Note that the light curve widths are used for comparisons within individual filters.
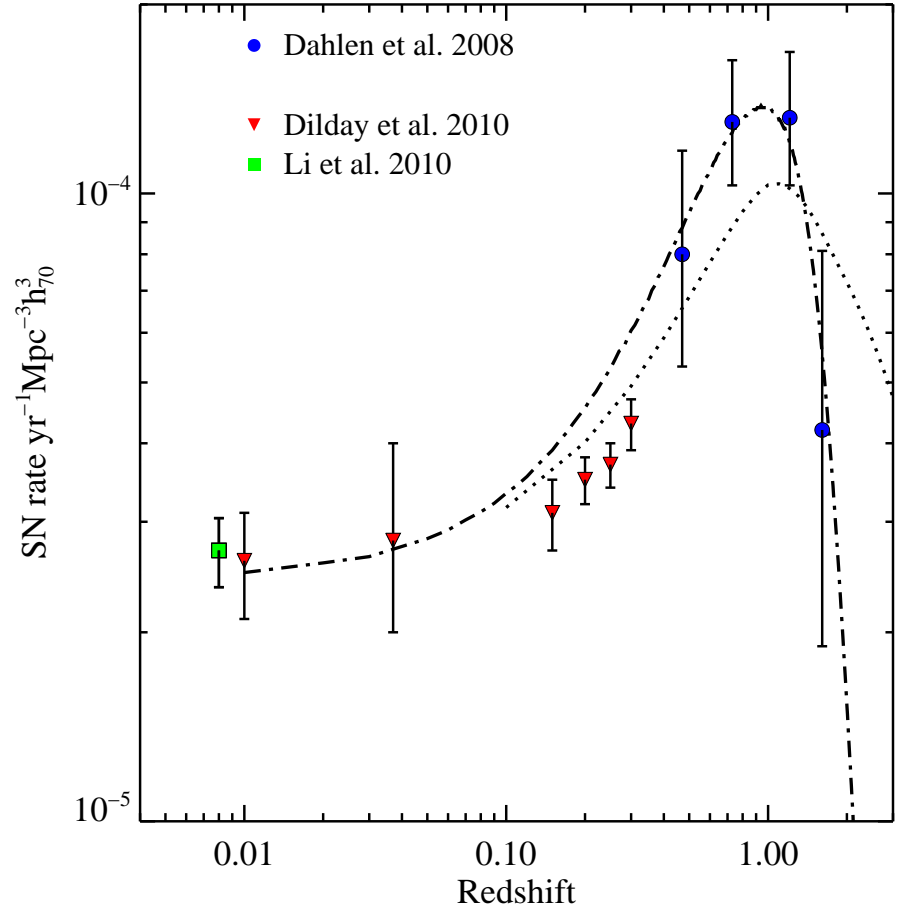
Figure 2: The evolution of the Type Ia supernova rate per unit volume as a function of redshift (data from [65]). The error bars reflect the statistical uncertainties per redshift bin. The highest redshift bin contains 3 objects. The increased rate with redshift follows the increased star formation rate observed in the universe. The two models [66, 67] show the effect of different progenitor life times. A long progenitor evolution towards a supernova (dash-dotted line) means that no SNe Ia are observed in the early universe. In the case of a shorter delay time (dotted line) the rate remains high at high redshifts (and large look-back times).
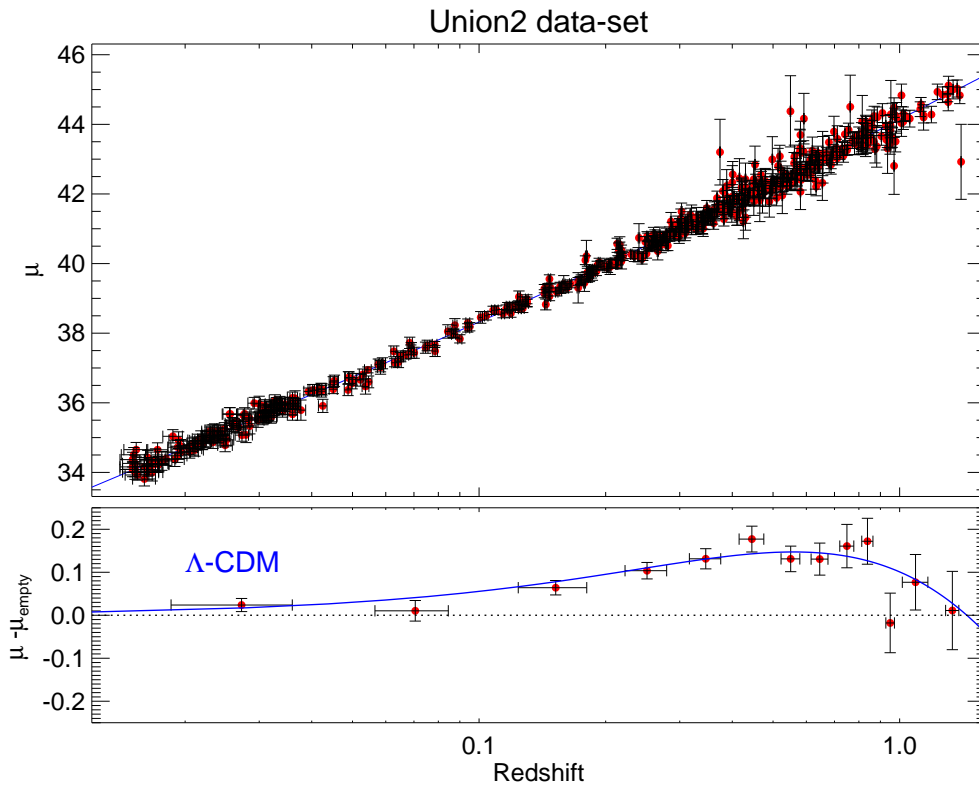
Figure 3: The Hubble diagram of Type Ia supernovae correlating distance modulus (μ) *vs.* redshift. The Union2 compilation [69] represents the currently largest SN Ia sample. The linear expansion in the local universe can be traced out to z<0.1. The Hubble constant sets the absolute level of the data, while it is irrelevant for the determination of Ω_Λ, which is a relative measurement (bottom panel). The distance relative to an empty universe model (μ_{empty}; $\Omega_M = \Omega_\Lambda = 0$) is shown in the lower panel. The data are binned for clarity in this diagram. The blue curve shows the expectation from the best fit ΛCDM model ($\Omega_M = 0.3, \Omega_\Lambda = 0.7$).
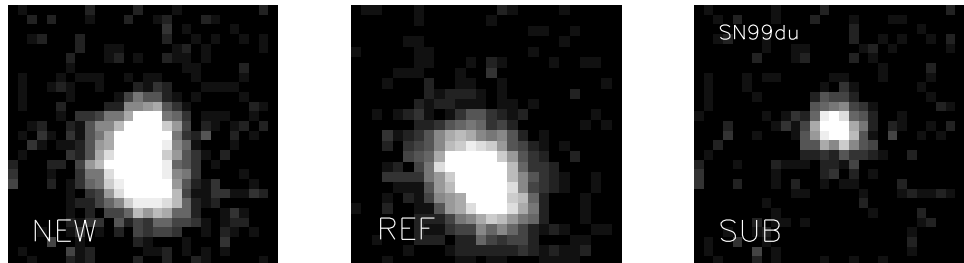
Figure 4: Detection principle for supernovae: images separated by between a few days and weeks are subtracted from each other (NEW - REF = SUB). In this case, g-band images used to detect SN 1999du ($z = 0.260$) in [73] are shown.

Ref	N_{SN}	Ω_M (flat)	w (constant, flat)	LC fitter
Astier *et al.* (2006)	115	$0.263^{+0.042}_{-0.042}\,^{+0.032}_{-0.032}$	$-1.023^{+0.090}_{-0.090}\,^{+0.054}_{-0.054}$	SALT
Wood-Vasey *et al.* (2007)	162	$0.267^{+0.028}_{-0.018}$	$-1.069^{+0.091}_{-0.093}\,^{+0.13}_{-0.13}$	MLCS2k2
	178	$0.288^{+0.029}_{-0.019}$	$-0.958^{+0.088}_{-0.090}\,^{+0.13}_{-0.13}$	SALT2
Kessler *et al.* (2009)	288	$0.307^{+0.019}_{-0.019}\,^{+0.023}_{-0.023}$	$-0.76^{+0.07}_{-0.07}\,^{+0.11}_{-0.11}$	MLCS2k2
	288	$0.265^{+0.016}_{-0.016}\,^{+0.025}_{-0.025}$	$-0.96^{+0.06}_{-0.06}\,^{+0.13}_{-0.13}$	SALT2
Amanullah *et al.* (2010)	557	$0.279^{+0.017}_{-0.016}$	$-0.997^{+0.050}_{-0.054}\,^{+0.077}_{-0.082}$	SALT2

Table 1: Cosmological parameters from the first year papers of SNLS, ESSENCE and SDSS and the Union2 sample, Refs. [69, 89, 96, 98]. The fits include lower redshift data as well as BAO and CMB information. A flat $w-$CDM model with constant w is assumed in all analysis (see text for more detail).
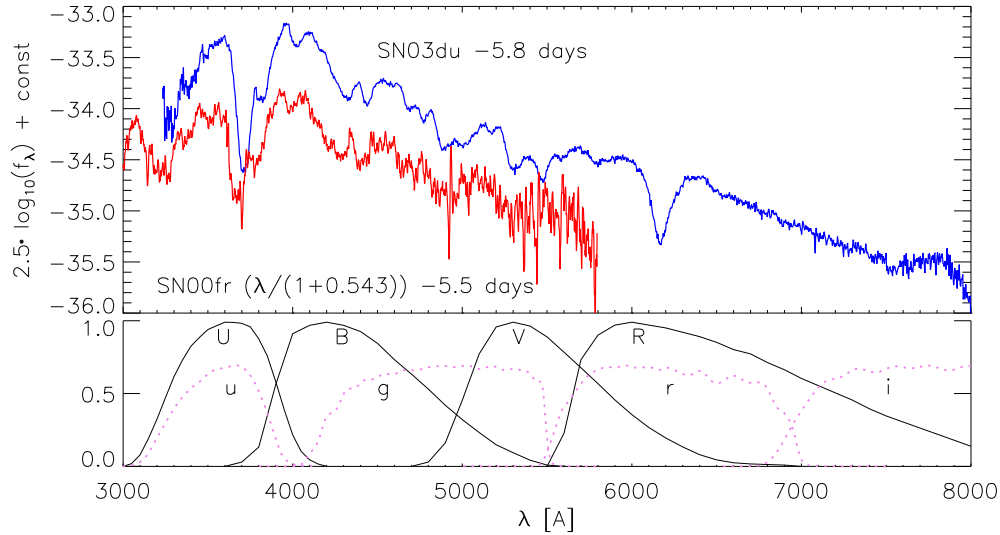
Figure 5: The observed spectrum of SN 2003du [74] compared with the restframe spectrum of SN 2000fr (z=0.543; [75]), both about 6 restframe days prior to B-filter maximum. The two spectra display remarkable similarities in the absorption and emission regions. Currently available data have not provided any evidence of clearly different spectral appearance of distant SNe Ia compared to their local counterparts indicating that there are no major changes in the explosion physics. The spectrum of the nearby supernova extends to much longer wavelengths, which are redshifted outside the observable window for the distant supernova, where the restframe UV region (not fully shown) is covered much more extensively. The bottom panel indicates the optical filter bands for the Johnson-Cousins UBVR system as well as the SDSS ugri filter set.
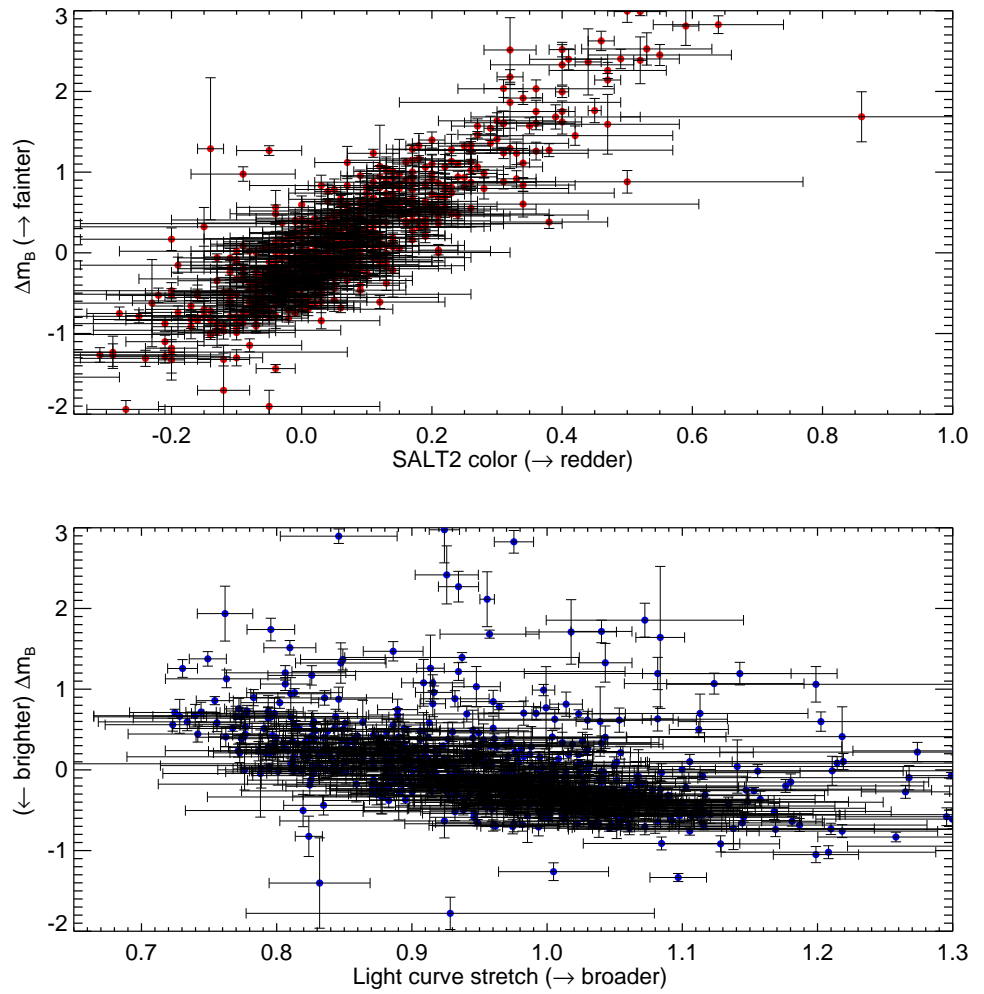
Figure 6: The color *vs.* luminosity (upper panel) and the light curve shape *vs.* luminosity (lower panel, after color corrections) correlations of Type Ia supernovae. Light curve fits to the restframe B filter observations of 685 SNe Ia [69] covering a redshift range from 0.025<z<1.4 are displayed. The clear correlations are used to correct the distances and provide a significant reduction in the scatter. It should be noted that the color has already been corrected for Milky Way reddening.
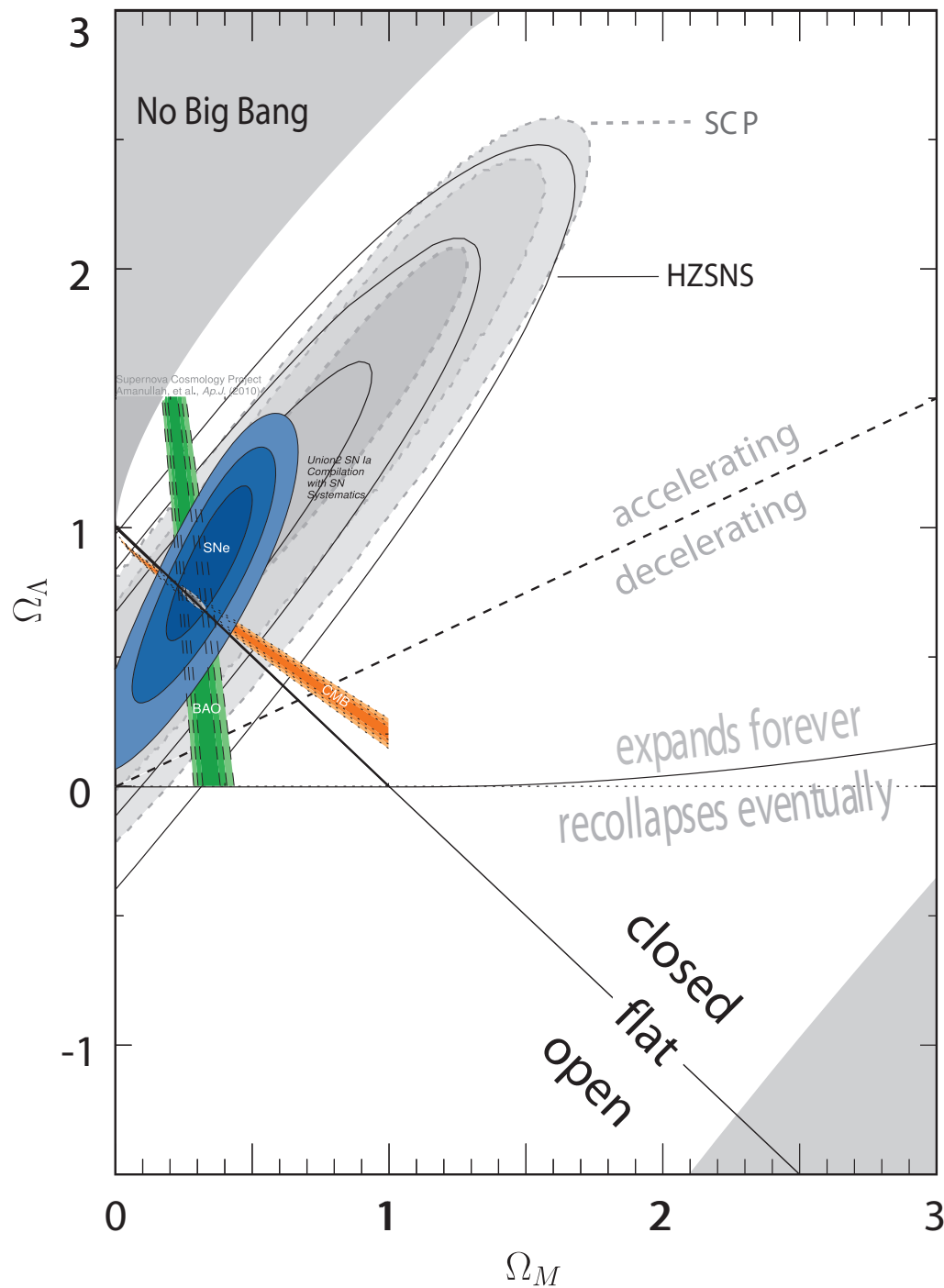
Figure 7: Confidence level regions in the $(\Omega_M, \Omega_\Lambda)$ parameter plane. The larger contours show the original results from the High-Z Supernova Survey (HZSNS; [15]) and the Supernova Cosmology Project (SCP; [16]). The blue areas correspond to the 68.3, 95.4 and 99.7% confidence limits of the Union2 compilation of SNe Ia [69]. Baryonic acoustic oscillations (BAO; green) and cosmic microwave background (CMB; orange) constraints from [93] and [94] are also
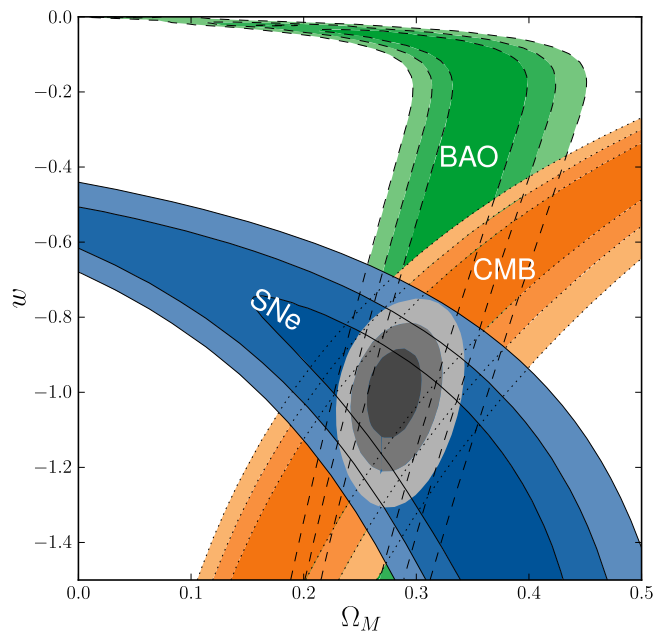
Figure 8: The current best constraints for a constant w are shown here. A cosmological constant (w=0) still is valid solution. The complementarity of the different methods is apparent. The supernova probability distribution is nearly perpendicular to the ones from the baryonic acoustic oscillations or the microwave background. Data taken from [69].
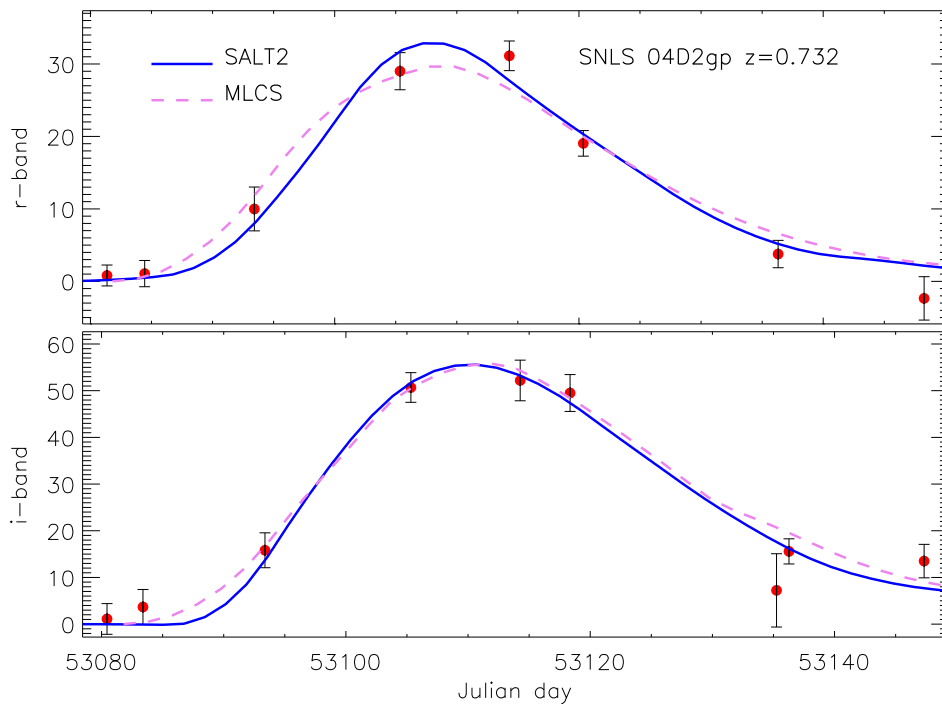
Figure 9: The differences incurred from using different light curve fitters is demonstrated here. The same $r-$ and i-filter observations (fluxes, not magnitudes) of the SNLS supernova 04D2gp (z=0.732) are approximated with the SALT2 and the MLCS2k2 fitters, two of the most used fitters at the moment. Small deviations in the $i-$filter fitting can be seen and are due to the different underlying templates used in the fitters and differences in how the colors are determined simultaneously.
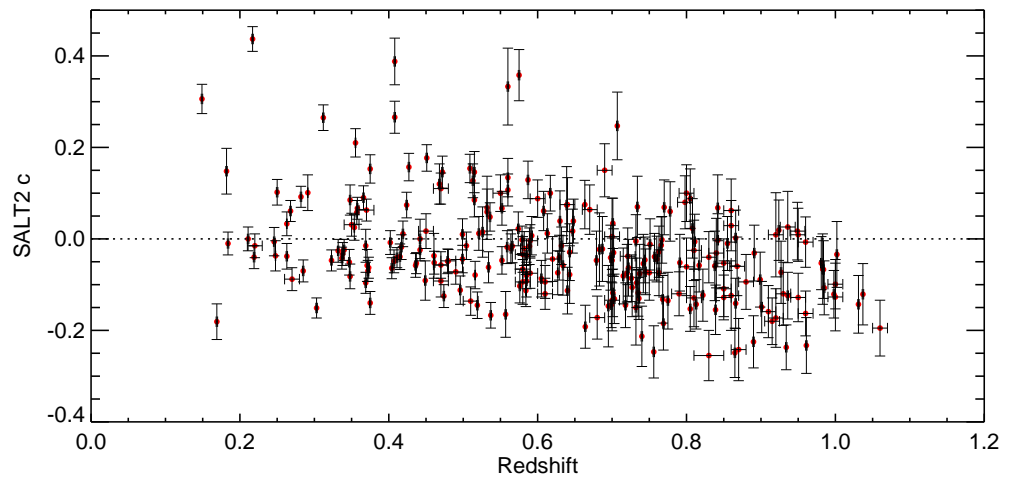
Figure 10: Fitted SALT2 color, c, vs redshift for the 3-year SNLS data-set [97]. There is strong evidence for a selection effect, with bluer supernovae being found at larger redshifts. Since bluer supernovae are intrinsically more luminous this effect can be explained as a selection driven by the magnitude limit of the spectroscopic follow-up.
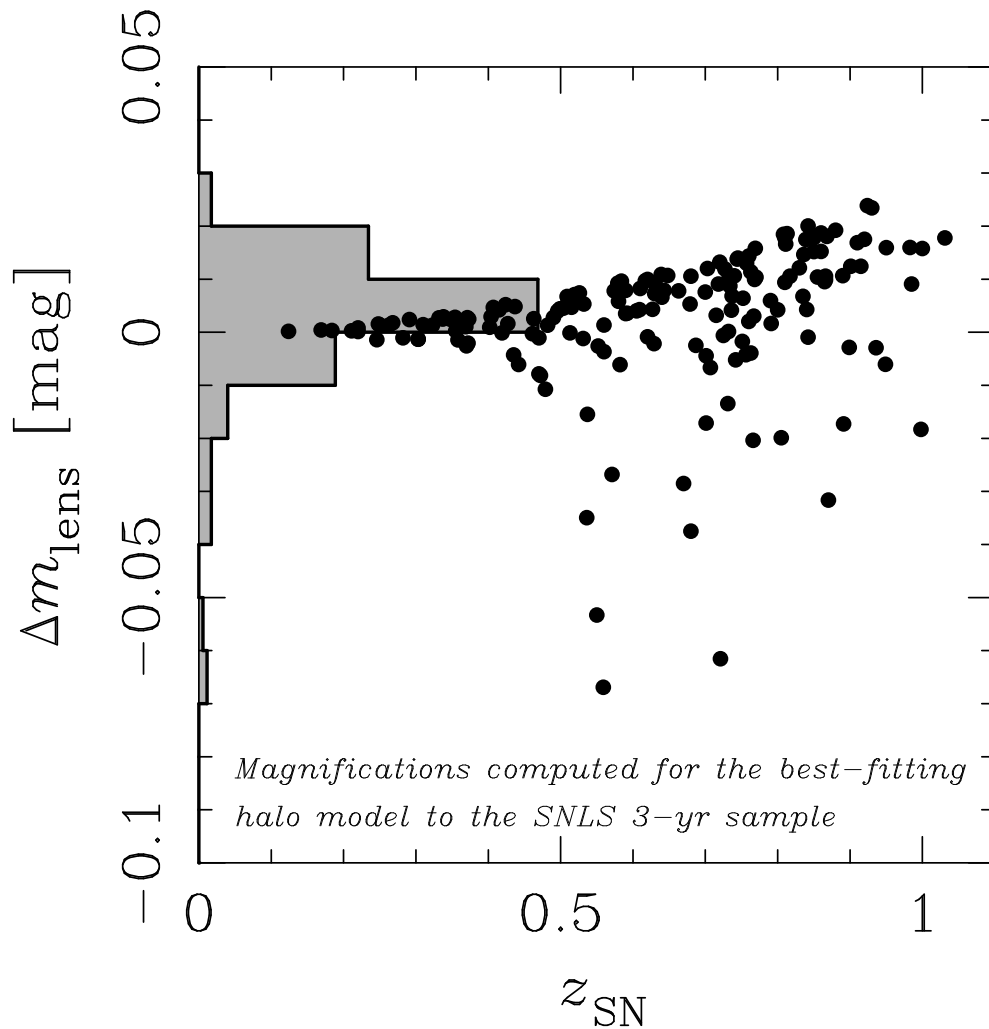
Figure 11: Magnification of SNe Ia in the 3-year SNLS data vs. redshift. Filled circles represent the estimated lensing magnification, Δm_{lens}, to individual Type Ia SNe, based on the best fit halo model from [135]. The effect grows with redshift, but the mean value is close to zero, as also indicated by the histogram on the side. Figure courtesy of Jakob Jönsson.
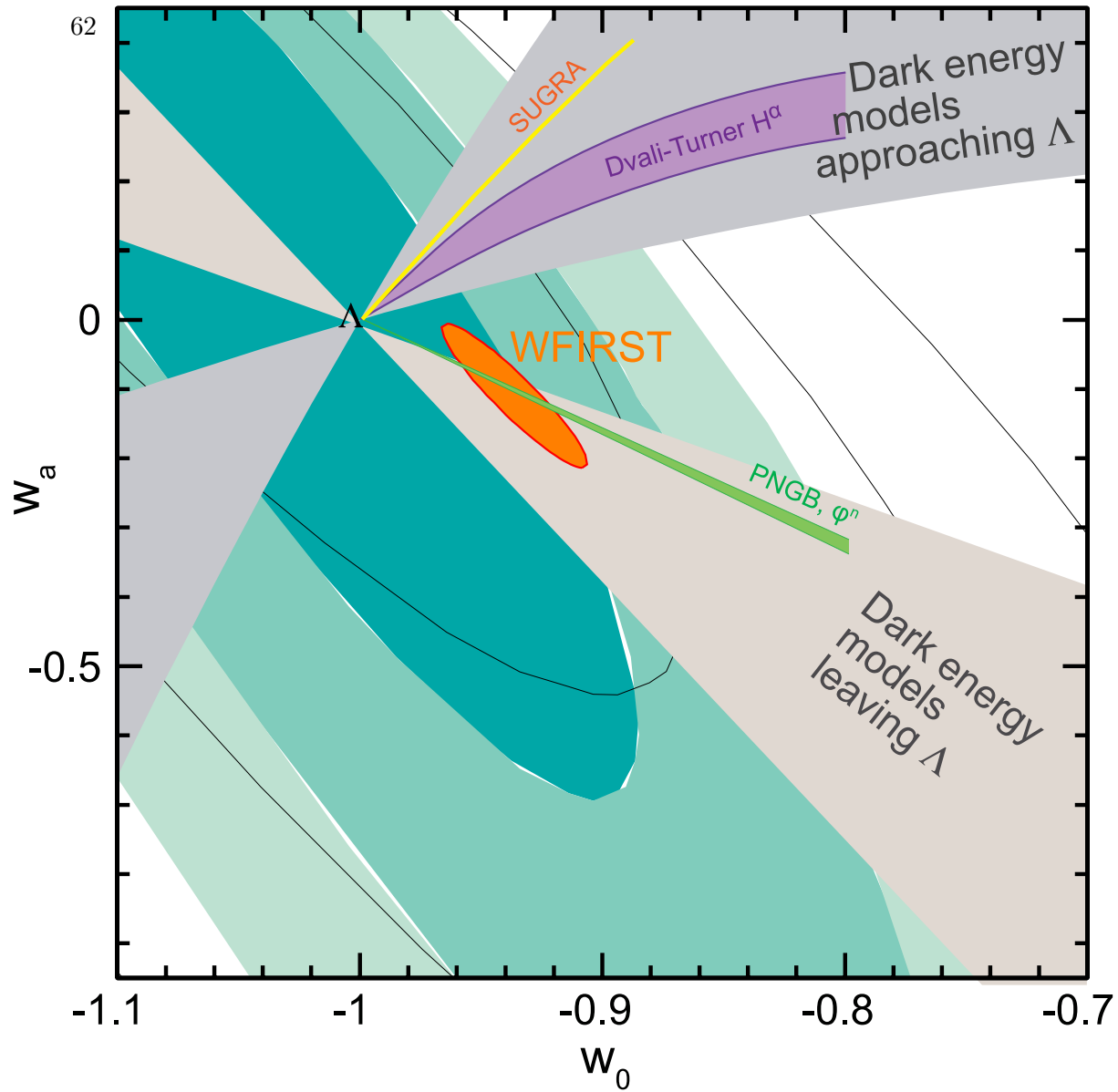
Figure 12: Projected 68% confidence region in the (w_0, w_a) plane for a planned satelite mission (Eric Linder, private communication) compared with the Union2 results. While the existing data cannot constrain a time-dependent w future missions have the promise to meaningful constrain this quantity. Figure adapted by Joel Johansson.